



1 Plateaus and jumps in the atmospheric radiocarbon record – Potential origin and value as
2 global age markers for glacial-to-deglacial paleoceanography, a synthesis

3
4

5 Michael Sarnthein¹⁾, Kevin Küssner²⁾, Pieter M. Grootes³⁾, Blanca Ausin⁴⁾, Timothy
6 Eglinton⁴⁾, Juan Muglia⁵⁾, Raimund Muscheler⁶⁾, Gordon Scholaut⁷⁾

7
8

9 1) Institute of Geosciences, University of Kiel, Olshausenstr. 40, 24098 Kiel, Germany,
10 michael.sarnthein@ifg.uni-kiel.de, (corresponding author)

11 2) Alfred-Wegener-Institut Helmholtz-Zentrum für Polar- und Meeresforschung,
12 Department for Marine Geology, 27570 Bremerhaven, Germany, kevin.kuessner@awi.de

13 3) Institute of Ecosystem Research, University of Kiel, Olshausenstr. 40, 24098 Kiel,
14 Germany, pgrootes@ecology.uni-kiel.de

15 4) Geological Institute, ETH Zürich, Sonneggstr. 5, 8092 Zuerich, Switzerland,
16 blanca.ausin@erdw.ethz.ch

17 5) College of Earth, Ocean and Atmospheric Sciences, Oregon State University, 104
18 CEOAS Administration Building, 101 SW 26th St, Corvallis, OR 97331, USA,
19 juanmuglia@gmail.com

20 6) Quaternary Sciences, Department of Geology Lund University, Sölvegatan 12, S-
21 223 62 Lund, Sweden, raimund.muscheler@geol.lu.se

22 7) Climate Dynamics and Landscape Evolution, GFZ German Centre for Geosciences,
23 Telegrafenberg, 14473 Potsdam, Germany, ScholautG@gmail.com

24
25
26



27 ABSTRACT

28 Changes in the geometry of ocean Meridional Overturning Circulation (MOC) are crucial in
29 controlling changes of climate and the carbon inventory of the atmosphere. However, the precise
30 timing and global correlation of short-term glacial-to-deglacial changes of MOC in different ocean
31 basins still present a major challenge. A possible solution is offered by the fine structure of jumps
32 and plateaus in the record of radiocarbon (^{14}C) concentration of the atmosphere and surface ocean
33 that reflects changes in atmospheric ^{14}C production as well as in the ^{14}C exchange between air
34 and sea and within the ocean. Boundaries of atmospheric ^{14}C plateaus in the ^{14}C record of Lake
35 Suigetsu, now tied to Hulu U/Th model-ages instead of optical varve counts, provide a
36 stratigraphic 'rung ladder' of ~30 age tie points from 29 to 10 ka for correlation with and dating of
37 planktic oceanic ^{14}C records. The age difference between contemporary planktic and atmospheric
38 ^{14}C plateaus gives an estimate of the global distribution of ^{14}C reservoir ages for surface waters of
39 the Last Glacial Maximum (LGM) and deglacial Heinrich Stadial 1 (HS-1), as shown by 19 planktic
40 ^{14}C records. Clearly elevated and variable reservoir ages mark both high-latitude sites covered by
41 sea ice and/or meltwater and upwelling regions. ^{14}C ventilation ages of LGM deep waters reveal
42 opposed geometries of Atlantic and Pacific MOC. Similar to today, Atlantic deep-water formation
43 went along with an estuarine inflow of old abyssal waters from the Southern Ocean up to the
44 northern North Pacific and an outflow of upper deep waters. Vice versa, ^{14}C ventilation ages
45 suggest a reversed MOC during early HS-1 and a ~1500 year long flushing of the deep North
46 Pacific up to the South China Sea, when estuarine circulation geometry marked the North Atlantic,
47 gradually starting near 19 ka. Elevated ^{14}C ventilation ages of LGM deep waters reflect a major
48 drawdown of carbon from the atmosphere. Inversely, the subsequent massive age drop and
49 change in MOC induced two major events of carbon release to the atmosphere as recorded in
50 Antarctic ice cores, shifts that highlight the significance of ocean MOC for atmospheric CO_2 and its
51 ^{14}C inventory. These new features of MOC and the carbon cycle offer a challenge to model
52 simulations that, in part because of insufficient spatial model resolution and reference data for
53 testing the model results, still poorly reproduce them.



54	LIST of CONTENTS
55	
56	1. INTRODUCTION – A THEORETICAL FRAMEWORK
57	1.1– <i>A variety of terms linked to the notion ‘^{14}C age’</i>
58	1.2– <i>Review of tie points used to fix calendar and reservoir ages in marine ^{14}C records</i>
59	1.3– <i>Items to be addressed in this synthesis</i>
60	
61	2. AGE TIE POINTS BASED ON ^{14}C PLATEAU BOUNDARIES
62	2.1– <i>A slight revision of absolute age control of the Suigetsu ^{14}C record</i>
63	2.2– <i>Uncertainties of age control (A chapter to be shifted to Suppl. Materials #1)</i>
64	
65	3. DISCUSSION
66	3.1– <i>Origin of short-term structures in the atmospheric ^{14}C record: Changes in cosmogenic ^{14}C production</i>
67	<i>versus changes in ocean dynamics</i>
68	3.2– <i>^{14}C plateau boundaries – A suite of narrow spaced age tie points (a ‘rung ladder’) to rate short-term</i>
69	<i>changes in marine sediment budgets, chemical inventories, and climate 29–10 cal. ka</i>
70	3.3– <i>Definition and origin of Zoophycos burrows: A key foe of high-resolution stratigraphy in Pleistocene</i>
71	<i>sediment records turned into an ally?</i>
72	3.4– <i>Empiric vs. model-based ^{14}C reservoir ages acting as tracer of past changes in surface ocean</i>
73	<i>dynamics</i>
74	3.5– <i>Plankton-based ^{14}C reservoir ages – A prime database to estimate past changes in the ^{14}C</i>
75	<i>ventilation age of deep waters, ocean MOC, and DIC for past states of the ocean</i>
76	3.5.1 • <i>Major features of meridional overturning circulation during LGM</i>
77	3.5.2 • <i>Major features of meridional overturning circulation during early HS-1</i>
78	3.5.3 • <i>Deep-Ocean DIC inventory</i>
79	
80	4. SOME CONCLUSIONS
81	
82	ACKNOWLEDGMENTS
83	
84	REFERENCES
85	
86	TABLE and FIGURE CAPTIONS
87	
88	Supplementary Figure Captions and Figures
89	



90 1. INTRODUCTION

91 1.1 A variety of terms linked to the notion ' ^{14}C age'

92 The ^{14}C concentration in the troposphere is mainly determined by ^{14}C production,
93 atmospheric mixing, moreover, air-sea gas exchange, and ocean circulation that vary over
94 time (e.g., Alves et al., 2018; Alveson et al., 2018). The ^{14}C content of living terrestrial
95 plants is in equilibrium with the atmosphere via processes of photosynthesis, respiration,
96 and accordingly, the ^{14}C of terrestrial plant remains in a sediment section directly reflects
97 the amount of radioactive decay, thus the time passed since the plant's death, and the ^{14}C
98 composition of the atmosphere during the time of plant growth.

99

100 Contrariwise, ^{14}C values of marine waters are cut off from cosmogenic ^{14}C production in
101 the atmosphere, hence depend on the carbon transfer at the air-sea interface and
102 transport and mixing of carbon in the ocean. For surface waters, the air-sea transfer is
103 relatively fast and effective involving a time span of ten years and less (e.g., Nydal et al.,
104 1998). Yet, vertical and horizontal water mixing results in surface ocean ^{14}C
105 concentrations differing from those in the contemporaneous atmosphere, expressed as
106 differential ^{14}C 'reservoir ages' (or 'reservoir effects' *sensu* Alves et al., 2018). These
107 'ages' reflect the local oceanography and are highly variable through time. Differences
108 may range from near zero up to values of more than 700 yr, in some regions up to 2500
109 yr, induced, for example, by old waters upwelled from below (e.g., Stuiver and Braziunas,
110 1993; Grootes and Sarnthein, 2006; Sarnthein et al., 2015). Apart from U/Th dated corals
111 (many papers on their reservoir age since Adkins and Boyle, 1997) the ^{14}C age of planktic
112 foraminifers is the most common tracer of surface water ages in marine sediments, a
113 rough estimate of the time passed since sediment deposition. Initially, marine geologists
114 were most interested in this 'simple' age value. Soon, however, they were confronted with



115 age inconsistencies that implied a series of unknowns, in particular the ^{14}C 'reservoir age'
116 that finally turned out to be a most valuable tracer of oceanography.

117

118 In turn, ^{14}C records of benthic carbonate particles in deep-sea sediments sum the time of
119 radioactive decay since their deposition with the apparent 'ventilation age' of the deep
120 waters in which they lived. Ventilation age is primarily the time span from the moment
121 when carbon dissolved in the (later) deep waters lost contact with the ^{14}C level of the
122 atmosphere and the somewhat reduced level of surface waters until the precipitation of
123 benthic carbonate. Details on the derivation of ventilation ages are given in Cook and
124 Keigwin (2015) and Balmer and Sarnthein (2018). In addition, however, ventilation ages
125 depict hardly quantifiable lateral admixtures of older and/or younger water masses,
126 moreover, ^{14}C -enriched organic carbon supplied by the biological pump, thus are called
127 'apparent'. Today, the apparent transit times of carbon dissolved in the deep ocean range
128 from a few hundred up to ~ 1800 ^{14}C yr found in upper deep waters of the northeastern
129 North Pacific (Matsumoto, 2007).

130

131 Over the last decades, it turned out that both the reservoir ages of surface waters and the
132 ventilation ages of deep waters present robust and high-resolution tracers essential for
133 drawing quantitative conclusions on past ocean circulation geometries, marine climate
134 change, and the processes that drive both past ocean dynamics and carbon budgets,
135 given the ages rely on a number of robust age tie points. Obtaining such tie points
136 presents a problem, since any attempt to date a deep-sea sediment record by means of
137 ^{14}C encounters a number of intricacies of how to disentangle (i) the effects of atmospheric
138 ^{14}C variations due to past changes in cosmogenic ^{14}C production and carbon cycle, still
139 hampered by the need for a generally accepted atmospheric reference record for the



140 period 14–50 ka, from (ii) depositional effects such as sediment hiatuses and winnowing,
141 differential bioturbational mixing depth, sediment transport by deep burrows, (iii) the
142 effects of ocean mixing resulting in reservoir and ventilation ages that change through time
143 and space (e.g., Alves et al. 2018; Grootes and Sarnthein, 2006), and (iv) from the final
144 target, quantitatively ‘pure’ ^{14}C ages due to radioactive decay.

145

146 By now, ^{14}C -based chronologies of deep-sea sediment records, used to constrain and
147 correlate the age of glacial-to-deglacial changes in ocean dynamics and climate on a
148 global scale, are often of unsatisfactory quality when they are based on (i) age tie points
149 spaced far too wide-spaced (e.g., on DO-events 1, 2, and 3 only for the time span 30–14
150 cal ka), (ii) disregarding atmospheric ^{14}C plateaus, (iii) the risky assumption of \pm constant
151 planktic ^{14}C reservoir ages and other speculative stratigraphic correlations/compilations,
152 and (iv) on ignoring small-scale major differences in low-latitude reservoir age. Likewise,
153 clear conclusions are precluded by an uncertainty range of 3–4 kyr sometimes accepted
154 for tie points during the glacial-to-deglacial period (Lisiecki and Stern, 2016), where
155 significant global climate oscillations occurred on decadal-to-centennial time scales as
156 widely shown on the basis of speleothem and ice core-based records (Steffensen et al.,
157 2008; Svensson et al., 2008; Wang et al., 2001).

158

159 Thus marine paleoclimate and paleoceanographic studies today focus on the continuing
160 quest for a high-resolution and global, hence necessarily atmospheric ^{14}C reference record
161 that is marked by abundant, narrow-standing tie points on the calibrated (cal.) age scale.
162 Such pertinent tie points are provided by a suite of reproducible ‘plateaus’ and ‘jumps’ that
163 mark the atmospheric ^{14}C record (Figs. 1 and S1; Sarnthein et al., 2007 and 2015; Bronk



164 Ramsey et al., 2012 and 2019; Scholaut et al., 2018; Umling and Thunnell, 2017), hence
165 form the basis of this synthesis.

166

167 *1.2 Review of tie points used to fix calibrated and reservoir ages in marine ¹⁴C records*

168

169 The tree ring-based calibration of ¹⁴C ages provides a master record of decadal changes
170 in atmospheric ¹⁴C concentrations back to ~14 cal. ka (Reimer et al., 2013 and 2019) with
171 floating sections beyond (from ~12.5–14.5 cal. ka and around 29–31.5 and 43 cal. ka;
172 Turney et al., 2010, 2017). The evolution of Holocene and late deglacial ¹⁴C ages with time
173 is not linear but reveals variations with numerous distinct jump (= rapid change) and
174 (short) plateau-shaped (slow or no change or even inversion) structures indicative of
175 fluctuations in atmospheric ¹⁴C concentration. Prior to 8500 cal. yr BP, various plateaus
176 extend over 400–600 cal. yr and beyond (Fig. 2). Given the quality of the tree ring
177 calibration data, these fluctuations can be considered real, suitable for global correlation
178 (Sarnthein et al., 2007, 2015; Sarnthein and Werner, 2018). Air-sea gas exchange
179 transfers the atmospheric ¹⁴C fluctuations into the surface ocean where they can provide
180 high-resolution tie points to calibrate the marine ¹⁴C record and marine reservoir ages
181 back to ~14 ka (via the so-called ¹⁴C wiggle match approach). In the near future, however,
182 it is unlikely that a continuous tree ring-based record will become available to trace such
183 atmospheric ¹⁴C variations further back, over the period 14–29 cal. ka crucial for the
184 understanding of last-glacial-to-interglacial changes in climate. Hence various other, less
185 perfect ¹⁴C archives have been employed for this period to tie past changes in
186 atmospheric ¹⁴C concentration/age to an ‘absolute’ or ‘calibrated’ (e.g., incremental) age
187 scale and to constrain the widely unknown evolution of ¹⁴C reservoir ages of surface
188 waters for various regions of the ocean.



189

190 Suites of ^{14}C ages of paired marine and terrestrial plant-borne samples, e.g. paired
191 planktic foraminifers and wood chunks, provide most effective but rarely realizable
192 absolute-age markers and reservoir ages of local ocean surface waters (Zhao and
193 Keigwin, 2018; Rafter et al., 2018; Schroeder et al., 2016; Broecker et al., 2004).
194 Likewise successful can be the alignment of ^{14}C -dated variations in downcore sea-
195 surface temperatures (SST) with changes in hydroclimate as recorded in age-
196 calibrated sedimentary leaf-wax hydrogen isotope (δD) records from ancient lakes
197 (Muschitiello et al., 2019), assumed to be synchronous. Further tie points are derived
198 from volcanic ash layers (Waelbroeck et al., 2001; Siani et al., 2013; Davies et al.,
199 2014), paired U/Th- and ^{14}C -based coral ages (e.g., Adkins and Boyle, 1997; Chen et
200 al., 2015), and the (fairly fragmentary) alignment of major tipping points in ^{14}C dated
201 records of marine SST and planktic $\delta^{18}\text{O}$ to the incremental age scale of climate events
202 dated in Greenland and Antarctic ice core records (Waelbroeck et al., 2011). Such well-
203 defined climate-age tie points, however, are wide-spaced in peak glacial-to-early
204 deglacial ice core records. Finally, various data compilations tentatively rely on the use
205 of multiple age correlations amongst likewise poorly dated marine sediment records, an
206 effort necessarily problematic.

207

208 In the absence of robust age tie points an increasing number of authors resort to ^{14}C
209 reservoir age simulations for various sea regions by ocean GCMs (e.g. Butzin et al., 2017;
210 Muglia et al., 2018) to quantify the potential difference between marine and atmospheric
211 ^{14}C dates during glacial-to-interglacial times. Considering the complexity of the ocean
212 MOC and the global carbon cycle it is not surprising that the results of a comparison of a



213 selection of robust empiric vs. simulated ^{14}C reservoir ages are not that encouraging yet
214 (as discussed further below).
215
216 Accepting a generally close link between ^{14}C concentrations in the troposphere and in the
217 surface ocean, the fine structure of planktic ^{14}C records with centennial-scale-resolution
218 provides far superior (though costly) evidence, similar to that of tree rings, to furnish a
219 series of age tie points with semi-millennial-scale time resolution for a global correlation of
220 glacial-to-deglacial marine sediment sections. These suites of tie structures can link the
221 marine sediment records to a reference suite of narrow-standing jumps and boundaries of
222 the apparent plateaus found in the atmospheric ^{14}C record of Lake Suigetsu (Bronk
223 Ramsey et al., 2012, 2019) provided that common ^{14}C variations are robustly identified in
224 both atmospheric and marine records. Prior to 14 cal. ka, the absolute age of these
225 atmospheric ^{14}C structures can be calibrated either by (microscopy-based) varve ages or
226 by a series of paired U/Th- and ^{14}C -based model ages correlated from the Hulu Cave
227 speleothem record (Bronk Ramsey, 2012 and 2019; Southon et al., 2012; Cheng et al.,
228 2018). The difference between these calibrations (Fig. 3) is discussed below. It is,
229 however, little important for both the correlation and the derivation of the time-varying
230 offsets in ^{14}C concentration of planktic sediments from coeval concentrations in the
231 atmospheric record, an offset derived from the average ^{14}C age difference between two
232 'coeval' planktic and Suigetsu ^{14}C plateaus correlated.
233
234 A basic philosophical controversy exists whether the apparent jump and plateau structures
235 in the Suigetsu and planktic ^{14}C records reflect real ^{14}C fluctuations or statistical noise. In
236 the 'null hypothesis' the ^{14}C values shaping plateaus of the calibration curve are regarded
237 as result of mere statistical scatter. Thus, the record of atmospheric ^{14}C ages against time



238 would form a simple continuous rise resulting from radioactive decay and the advance of
239 time, such as suggested by a fairly straight progression of the highly resolved deglacial
240 Hulu Cave ^{14}C record plotted vs. U/Th ages (Southon et al., 2012; Cheng et al., 2018).
241
242 This null hypothesis is contradicted by the ‘master record’ of tree ring data (Fig. 2; Reimer
243 et al., 2013 /2020). Unequivocally it shows fluctuations in atmospheric ^{14}C concentration
244 on the order of 2–3 % over the last 10 kyr (Stuiver and Braziunas, 1993) and even larger
245 back to ~14 ka (Reimer et al., 2013, 2020). Though not resolved in speleothem data these
246 plateau/jump structures are real and widely reproducible in marine sediment records.
247 Under glacial and deglacial low- CO_2 conditions beyond 14 ka, when climate and ocean
248 dynamics were less constant than during the Holocene, atmospheric ^{14}C fluctuations were,
249 most likely, even stronger than those reported by Stuiver and Braziunas and ^{14}C plateaus
250 and jumps accordingly larger.
251
252 Thus, the age-defined plateaus and jumps in the Suigetsu atmospheric ^{14}C calibration
253 curve may most likely be regarded as a suite of ‘real’ structures, extending the tree ring
254 record for Holocene and B/A-to-Early Holocene times (Fig. 2) into early deglacial and LGM
255 times. In part the plateau/jump structures may be linked to changes in cosmogenic ^{14}C
256 production, as possibly shown in the ^{10}Be record (Fig. 4; based on data of Adolphi et al.,
257 2018), and – presumably more dominant – to short-term changes in ocean mixing and the
258 carbon exchange between ocean and atmosphere, the latter crucial, since the carbon
259 reservoir of the ocean contains up to 60 (preindustrial) atmospheric carbon units (Berger
260 and Keir, 1984). The apparent contradiction with the smooth Hulu Cave ^{14}C record
261 (Southon et al., 2012; Cheng et al., 2018) may possibly be explained by (i) the Hulu Cave
262 speleothem precipitation system acting as a low-pass filter for fluctuating atmospheric ^{14}C



263 concentrations (statistical tests of Bronk Ramsey et al., pers. comm. 2018), (ii) to a very
264 limited degree by the obvious scatter in the Suigetsu data that, however, appears
265 insufficient to feign plateaus in view of the evidence based on tree ring based plateaus
266 (Fig. 2). The filter for Hulu data possibly led to a sweeping loss especially of short-lived
267 structures in the preserved atmospheric ^{14}C record, though some remainders indeed were
268 preserved in the ^{14}C records of Hulu Cave (Fig. 1). So we rather trust in the amplitude of
269 Suigetsu ^{14}C structures, but trust in the timing of Hulu Cave data as discussed below.

270

271 Like a ‘rung ladder’ the age-calibrated suite of ^{14}C plateau boundaries and jumps is suited
272 for tracing the calibrated age of numerous plateau boundaries in glacial-to-deglacial
273 marine ^{14}C records likewise densely sampled. Moreover, one may record the offset of
274 planktic ^{14}C ages from paired atmospheric ^{14}C ages that is the planktic reservoir age, for
275 each single ^{14}C plateau (Sarnthein et al., 2007, 2015). For the first time, this suite of tie
276 points may facilitate a precise temporal correlation of all sorts of changes in surface and
277 deep-water composition on a global scale, crucial for a better understanding of past
278 changes in ocean and climate dynamics.

279

280 Over the time span 14–40 ka, the Suigetsu record of optical varve counts (Schlolut et al.,
281 2018) presents a rare means of age calibration of terrestrial and marine sediment records
282 being based on an incremental age scale similar to that of ice cores (e.g. Svensson et al.,
283 2008). In the crucial sediment sections of the Last Glacial Maximum (LGM) and deglacial
284 Heinrich Stadial 1 (HS-1), however, the degree of varve quality/perceptibility in the
285 Suigetsu profile is highly variable (Fig. 5), a problem met by Schlolut (2018) who
286 developed a special computer program to derive Suigetsu calendar ages from varve
287 counts. Nonetheless the interpolated varve counts have limited accuracy and precision. To



288 further improve the chronology the varve data were combined with Hulu Cave-based U/Th-
289 based model ages employed in this paper (Bronk Ramsey et al., 2012). The different age
290 models, however, do not affect our conclusions on planktic reservoir ages.

291

292 *1.3 Items to be addressed in this synthesis*

293

294 (1) The purely varve-based chronology of ^{14}C plateau boundaries previously employed for
295 the Suigetsu record (Sarnthein et al., 2015) may be incomplete in view of broad poorly
296 laminated sediment sections interpolated in Suigetsu sediment cores, recently recorded by
297 Scholaut et al. (2018). As compared to a U/Th-based age model (Bronk Ramsey et al.
298 2012; Cheng et al., 2018) many hundred years appear to have been missed. Thus, the
299 value of different age calibrations needs to be re-evaluated.

300

301 (2) In view of most recent findings on the quality of varve counts (Fig. 5; Scholaut et al.,
302 2018) our suite of tie points is now extended from 23 to 27/29 cal. ka. The calibrated-age
303 uncertainties of ^{14}C plateau boundaries and jumps in the redefined Suigetsu record
304 (Bronk-Ramsey et al., 2012, 2019; Sarnthein et al., 2015) and their correlatives in ocean
305 sediment cores, values crucial for any accurate correlation of these tie points to possibly
306 underlying ocean events over the period 10–27/29 cal. ka, are now discussed in
307 Supplement Text no. 1.

308

309 (3) Our set of records of marine ^{14}C reservoir ages (Sarnthein et al. 2015) has now been
310 amended by several records from the Southern Hemisphere (Balmer et al., 2016 and
311 2018; Küssner et al., 2017, and in prep.) and northeast Atlantic (Ausin et al., 2019 and in
312 prep.). In total, 18 (LGM) / 19 (HS-1) empiric records plus 3 wood chunk-based records



313 (e.g. Broecker et al., 2004; Zhao et al., 2018) now depict the spatial and temporal variation
314 of past ^{14}C reservoir ages of surface waters for different ocean regions.

315

316 (4) In the discussion we will compare our local reservoir ages with independent LGM
317 estimates of surface water ^{14}C reservoir ages simulated by the GCM of Muglia et al.
318 (2018). Differences between the results may help to constrain potential caveats in the
319 boundary conditions and fine structure of model simulations.

320

321 (5) We discuss some habitat- and season-specific ^{14}C reservoir ages characteristic of
322 different planktic foraminifera species, ages that monitor for past changes in the local
323 geometry of surface ocean dynamics (Sarnthein and Werner, 2018).

324

325 (6) Finally, we refer to ^{14}C reservoir and ventilation ages of surface and deep waters that
326 form a robust tracer of circulation geometries and the dissolved inorganic carbon (DIC) in
327 different basins of the ocean (Sarnthein et al., 2013). The estimates provide crucial
328 insights into the origin of past changes in the global carbon cycle from glacial to
329 interglacial times, an important correlative to model simulations.

330

331 2. AGE TIE POINTS BASED ON ^{14}C PLATEAU BOUNDARIES

332 2.1 *A slight revision of absolute age control of the Suigetsu ^{14}C record*

333

334 Originally, we based the chronology of ^{14}C plateau boundaries in the Suigetsu record
335 (Sarnthein et al., 2015) on a scheme of varve counts by means of light microscopy of thin
336 sections (Bronk Ramsey et al., 2012; Schlolaut et al., 2018). In parallel, varve-based age
337 estimates have been derived from counting various elemental peaks in μXRF data,



338 interpreted as seasonal signals (Marshall et al., 2012). In general, the results obtained
339 from these two independent counting methods and their interpolations widely support each
340 other. The microscopy-based counts ultimately formed the backbone of a high-resolution
341 chronology obtained by tying the Suigetsu ^{14}C record to the U/Th based time scale of the
342 Hulu cave ^{14}C record (Bronk Ramsey et al., 2012). Recently the scheme of varve counts
343 was revisited by Scholaut et al. (2018) who showed that Suigetsu varve preservation is
344 fairly high both over late glacial Termination I and prior to ~32 ky BP. However, it is fairly
345 poor over large parts of the LGM and HS-1, from ~15 - ~32 cal ka (17.3-28.5 m c.d. in Fig.
346 5), where less than 20-40 % of the annual layers expected from interpolation between
347 clearly varved sections are distinguished by microscopy per 20 cm sediment section. The
348 varve count using μXRF data (Marshall et al., 2012) can distinguish subtle changes in
349 seasonal element variations, which are not distinguishable in thin section microscopy,
350 hence results in higher varve numbers, for example, during early deglacial-to deglacial
351 times (Fig. 3). Yet, some subtle variations are difficult to distinguish from noise, thus also
352 introduce a degree of uncertainty to the μXRF -based counts. Thus the results deduced
353 from either counting method are subject to uncertainties, as shown by error estimates that
354 rise with increased varve age in Fig. 5.

355

356 In addition, Bronk Ramsey et al. (2012) established a time scale based on ^{14}C wiggle
357 matching to U/Th dated ^{14}C records of the Hulu Cave and Bahama speleothems. In part,
358 this calibrated (cal.) age scale was based on Suigetsu varve counts, in part on the
359 prerequisite of the best-possible fit of a pattern of low-frequency ^{14}C concentration
360 changes obtained from Suigetsu und Hulu Cave within the uncertainty envelope of the
361 Hulu 'Old / Dead Carbon Fraction' (OCF/DCF) of ^{14}C concentration. The uncertainty of this
362 model is debatable while the character of the Hulu DCF and thus, its uncertainty back in



363 time is still incompletely understood. We surmise that the U/Th-based age model of
364 Suigetsu may suffer from the wiggle matching of atmospheric ^{14}C ages of Lake Suigetsu
365 with ^{14}C ages of the Hulu Cave (Southon et al., 2012) in case of major short-term changes
366 in the memory effect of soil organic carbon in carbonate-free regions of the cave. These
367 carbonate-based ages may have been influenced far more strongly by short-term changes
368 in the local DCF than assumed, as suggested by major variations in a paired $\delta^{13}\text{C}$ record,
369 that reach up to 5 ‰, mostly subsequent to short-term changes in past monsoon climate
370 (Kong et al., 2005). Thus Hulu ^{14}C ages cannot directly be set equal to atmospheric ^{14}C
371 ages under the assumption of a constant OCF/DCF (Southon et al. 2012; Cheng et al.,
372 2018), a caveat that hampers the age model correlation between Hulu and Suigetsu
373 records. It turns out, U/Th-based model ages of ^{14}C plateau boundaries are much higher
374 than the microscopy-based varve ages over HS-1 and LGM we used thus far, a difference
375 accumulating from ~200 yr near 15.3 cal. ka to ~600 near 17 ka and 2000 yr near ~29 ka
376 (Fig. 3) and finally accepted by means of independent evidence shown below.

377

378 To calibrate the age of thirty ^{14}C plateau boundaries with the ‘best possible’ cal. time
379 scale we compared the results of the two timescales independently deduced from
380 varve counts with those of the U/Th-based model age scale using as test case the
381 base of ^{14}C Plateau 2b. In contrast to 16.4 cal. ka suggested by optical varve counts,
382 the XRF-based varve counts suggest an age of ~16.9 cal. ka (Marshall et al., 2012;
383 Schlolaut et al., 2018). Most important, this estimate matches closely that of 16.93 ka
384 on the U/Th-based time scale, a robust argument supporting the latter age scale (Fig.
385 1). Moreover, different from the microscopy-based varve age scale the U/Th model
386 time scale is further corroborated by a decent match with the ages of Mono Lake at 34



387 ka and Laschamp at 41 ka independently dated by other methods. We therefore chose
388 the U/Th model age scale to calibrate the age of ^{14}C boundaries.
389
390 The U/Th-based cal. ages result in reasonable stratigraphic correlations of millennial-scale
391 events in paleoceanography. Fig. 6 displays potentially correlative events of peak glacial
392 and deglacial change independently dated by means of annual-layer counts and/or U/Th
393 ages in ice cores and stalagmites (Table 2). As outlined below, atmospheric ^{14}C plateaus
394 may largely result from changes in air-sea gas exchange, and in turn, from changes in
395 ocean ventilation. A suite of deglacial ^{14}C plateaus indeed displays a temporal match with
396 major deglacial events in ocean degassing of CO_2 (Marcott et al., 2014) (Table 2 and Fig.
397 6). Also, short-term North Atlantic warmings matched three ^{14}C plateaus each during the
398 peak glacial and earliest deglacial times, similar to that at the end of HS-1.
399
400 In view of the recent revision of time scales (Schlölaut et al., 2018; Bronk Ramsey et al.,
401 2019) we extended our plateau tuning and now also defined the boundaries and age
402 ranges of ^{14}C plateaus and jumps for the interval ~23–27/29 cal. ka, which results in a total
403 of ~30 atmospheric age tie points for the time span 10.5–29 cal. ka (Fig. 1; summary in
404 Table 1; following the rules of Sarnthein et al., 2007 and 2015). Prior to 25 cal. ka, the
405 definition of ^{14}C plateaus somewhat suffered from an enhanced scatter of raw ^{14}C values
406 of Suigetsu. -- In addition to visual inspection, the ^{14}C jumps and plateaus were also
407 defined with higher statistical objectivity by means of the first-derivative of all trends in the
408 ^{14}C age-to-calendar age relationship (or –core depth relationship, respectively) by using a
409 running kernel window (Sarnthein et al., 2015).
410
411 Note, any readjustment of the calendar age of a ^{14}C plateau boundary does not entail any



412 change in ^{14}C reservoir ages afore deduced for surface waters by means of the plateau
413 technique (Sarnthein et al., 2007, 2015), since each reservoir age presents the simple
414 difference in average ^{14}C age for one and the same ^{14}C plateau likewise defined in both
415 the Suigetsu atmospheric and planktic ^{14}C records of marine surface waters, independent
416 of the precise position of this plateau on the calendar age scale.

417

418 *2.2 Uncertainties of age control (Chapter to be presented as Suppl. Text #1)*

419

420 Rough estimates of uncertainty and aspects of analytical quality were published by
421 Sarnthein et al. (2007, 2015). We now focus on uncertainties tied to the calendar age
422 definition for each ^{14}C plateau boundary both in the Suigetsu atmospheric and the
423 various marine sediment records (Table 1). To recap, an age/sediment section is
424 formally defined as containing a ' ^{14}C plateau', when ^{14}C ages show almost constant
425 values with an overall gradient of <0.3 to <0.5 ^{14}C yr per cal. yr (based on visual
426 description and/or statistical estimates by means of the 1st derivative of all
427 downcore changes in the ^{14}C age – calendar age relationship; Sarnthein et al., 2015)
428 and a variance of less than ± 100 to ± 300 ^{14}C yr, and up to 500 ^{14}C yr prior to 25 cal. ka.
429 Here ^{14}C ages form a plateau-shaped scatter band with up to 10% outliers, that
430 extends over more than 300 cal. yr in the Suigetsu record and/or equivalent sections of
431 marine sediment depth (following rules defined by Sarnthein et al., 2007).

432

433 On visual inspection a plateau boundary is assigned to the break point between the low
434 to zero or reversed slope of a ^{14}C plateau and the normally high regression slope of the
435 ^{14}C concentration jump that separates two consecutive plateaus (Figs. 1 and S1). More
436 precisely, a boundary marks the point, where the ^{14}C curve exceeds the scatter band of



437 the plateau either crossing the upper or lower envelope line. Thus the boundary is
438 chosen about halfway between the last ^{14}C age within a plateau band and the next
439 following age outside the scatter band (Figs. 1 and 2). Both on the previously varve-
440 based and the now U/Th-based model age scale (Bronk Ramsey et al., 2012) most ^{14}C
441 dates of the Lake Suigetsu section are spaced at intervals of $10\text{--}60\text{ yr}$ from 10 to 15
442 cal. ka and ones of 20–140 yr between 15 and 29 cal. ka (Fig. 1). Thus the uncertainty
443 of a plateau boundary age assigned halfway between two ^{14}C ages nearby inside and
444 outside a plateau's scatter band would, on average, amount to $\pm 10\text{--}\pm 70$ cal. yr.

445

446 In principle, the calendar age uncertainties of marine ^{14}C plateau boundaries are
447 treated likewise: After being tuned to those in the Suigetsu ^{14}C record, the uncertainties
448 are deduced for the position of all plateaus of a suite within the uncertainty envelope of
449 the U/Th model-based age calibration. Hence the estimates of total age uncertainty
450 present the square root of the squared uncertainty of the calibrated age of each
451 plateau boundary at Suigetsu plus that of the marine record, where variable depth
452 spacing of ^{14}C ages is converted into average time spans.

453

454 3. DISCUSSION

455 *3.1 Origin of short-term structures in the atmospheric ^{14}C record: Changes in cosmogenic* 456 *^{14}C production versus changes in ocean dynamics*

457

458 Besides possible climate influences, variations in ^{10}Be deposition in ice cores reflect past
459 changes in ^{10}Be production as a result of changes in solar activity and the strength of the
460 Earth's magnetic field (Adolphi et al., 2018). Correspondingly, the changes in ^{10}Be also
461 reflect past changes in the cosmogenic production of ^{14}C . If we accept to omit



462 assumptions on the modulation of past ^{14}C concentrations by changes in the global carbon
463 cycle over last glacial-to-deglacial times we can calculate the atmospheric ^{14}C changes
464 with a carbon cycle model and convert it into ^{14}C ages (Fig. 4), although being aware that
465 carbon cycle changes are prominent and necessarily modify the ^{10}Be -based ^{14}C record if
466 included correctly into the modeling. Between 10 and 13.5 cal. ka, the modeled ^{14}C record
467 displays a number of plateau structures that show a decent match with Suigetsu-based
468 atmospheric ^{14}C plateaus. Between 15 and 29 cal. ka, however, ^{10}Be -based ^{14}C plateaus
469 are far more rare and/or less pronounced, except for a distinct equivalent of Plateau 6a,
470 that is, most plateaus are far shorter than those displayed in the suite of atmospheric ^{14}C
471 plateaus of Lake Suigetsu (e.g., plateaus near to the top 2a, 2b, and top 5a of Suigetsu
472 plateaus). On the whole, the structures show little coherence, thus indicating that any
473 direct relationship between variations in cosmogenic ^{14}C production and the Suigetsu
474 plateau record is obscured by the carbon cycle, uncorrected climate effects on the ^{10}Be
475 deposition and/or noise in the ^{14}C data.

476

477 On the other hand, three long ^{14}C plateaus (no. 2a, 1, and Top YD) that dominate the ^{14}C
478 record during deglacial times (Table 2 and Fig. 6) may be ascribed to coeval brief periods
479 being marked by a short-term major rise in global ocean degassing (Marcott et al. 2014).
480 We thus assume that these events which induced a rapid rise in ^{14}C depleted atmospheric
481 CO_2 may be linked to a variety of fast changes such as that of sea ice cover in the
482 Southern Ocean and/or changes in the salinity and buoyancy of surface waters in high
483 latitudes. These factors control upwelling and meridional overturning of deep waters, in
484 particular, as found in the Southern Ocean (Chen et al., 2015) and/or North Pacific (Rae et
485 al. 2014, Gebhardt et al., 2008). Such events of changes in MOC geometry and intensity
486 may be responsible for ocean degassing and the ^{14}C plateaus as outlined below.



487

488 In an extreme case, ventilation ages in the Southern Ocean near New Zealand (SO213-76
489 in Fig. S4; Küssner et al., 2019, in prep.) drop from 4000 years (~60 % of the
490 contemporaneous level of past atmosphere 1.4 'Fraction of Modern Carbon' [FMC] at that
491 time leading to $1.4 \times 0.6 = 0.84$ FMC) to 1000 years (equal to 88 % of past atmosphere
492 FMC) around 18 cal. ka with an otherwise constant atmospheric ^{14}C of 1.4 FMC. This
493 implies an increase to $1.4 \times 0.88 = 1.232$ FMC of local deep ocean ^{14}C at this site. The
494 concentration difference of ~0.4 FMC means a major ^{14}C shift in DIC at that very MOC key
495 region of the deep Southern Ocean (Rae and Broecker, 2018) over 200 yr. This enhanced
496 mixing of the Southern Ocean and a similar mixing event in the North Pacific (MD02-2489;
497 Fig. S4) may have triggered – with phase lag – two trends in parallel, (1) a rise in
498 atmospheric CO_2 , in part abrupt (*sensu* Chen et al., 2015; Menviel et al., 2018), and (2) a
499 gradual enrichment in ^{14}C depleted atmospheric carbon, reflected as ^{14}C plateau.

500

501 By contrast, there is little information for the origin of peak glacial ^{14}C plateaus no. 4 to 11.
502 Some of them may possibly be tied to major short-term warmings / MOC modifications in
503 the North Atlantic such as that during plateau 'YD', during plateaus no. 3 (at the onset of
504 Antarctic warming; e.g., Kawamura et al., 2007) and no. 8 (on the U/Th-based age scale;
505 Table 2). These warmings were probably linked to enhanced overturning and short-term
506 degassing of ^{14}C depleted deep waters in the North Atlantic. However, the causal links of
507 various further peak glacial plateaus to events in ocean MOC still remain to be uncovered.

508

509 *3.2 ^{14}C plateau boundaries – A suite of narrow-spaced age tie points to rate short-term*
510 *changes in marine sediment budgets, chemical inventories, and climate 29–10 cal. ka*

511



512 In continuation of previous efforts (Sarnthein et al., 2007 and 2015) the tuning of high-
513 resolution ^{14}C records of ocean sediment cores to the new age-calibrated atmospheric ^{14}C
514 plateau boundaries now makes it possible to establish a 'rung ladder' of ~30 age tie points
515 covering the time span 29 – 10.5 cal. ka. On a global scale these tie points show a time
516 resolution of several hundred to thousand years, now used to constrain the chronology
517 and potential leads and lags of any kind of event that occurred during peak glacial and
518 deglacial times (Fig. 1). The locations of the 18(20) cores are shown in Fig. S2. The time
519 histories of the benthic and planktic reservoir ages are summarized in Figs. S3 and S4 and
520 the information these provide is discussed below.

521

522 In particular, five examples show the power and value of additional information obtained
523 by means of the ^{14}C plateau-tuning method. (i) Signals of the onset of northern
524 hemisphere deglaciation can now be distinguished in detail from the subsequent beginning
525 of deglaciation in the southern hemisphere (Kawamura et al., 2007; Küssner et al., 2019 in
526 prep.). (ii) A multicentennial-scale phase lag has been specified for the end of the Antarctic
527 Cold Reversal (ACR) vs. the onset of the Younger Dryas cold spell (Küssner et al., 2019 in
528 prep.), a finding important to further constrain the details of 'bipolar see-saw' (Stocker and
529 Johnsen, 2003). (iii) Signals of deep-water formation in the subpolar North Pacific can now
530 be separated from signals originating in the North Atlantic (Rae et al. 2014; Sarnthein et
531 al., 2013). In this way we now can specify and tie major short-lasting reversals in Atlantic
532 and Pacific MOC on a global scale. (iv) Signals of deglacial meltwater advection can now
533 be distinguished from short-term interstadial warmings in the northern subtropical Atlantic,
534 which helps to locate meltwater outbreaks far beyond the well-known Heinrich belt of ice-
535 rafted debris (Balmer and Sarnthein, 2018). (v) As outlined above, the timing of marine ^{14}C
536 plateaus can now be compared in detail with that of deglacial events of the atmospheric



537 CO₂ rise independently dated by means of ice core-based stratigraphy (Table 2; Fig. 6).
538 These linkages enable a better understanding of deglacial changes in deep-ocean MOC
539 once the suite of ¹⁴C plateaus has been properly tuned at any particular ocean site.
540
541 Furthermore, the refined scale of age tie points reveals unexpected details for changes in
542 the sea ice cover of high latitudes as reflected by anomalously high ¹⁴C reservoir ages
543 (e.g. north of Iceland and near to the Azores Islands) and for the evolution of Asian
544 summer monsoon in the northern and southern hemisphere as reflected by periods of
545 reduced sea surface salinity (e.g., Sarnthein et al., 2015; Balmer et al., 2018). Finally, the
546 plateau-based high-resolution chronology has led to a detection of numerous millennial-
547 scale hiatuses (e.g., Sarnthein et al., 2015; Balmer et al., 2016; Küssner et al., 2019 in
548 prep.) previously undetected by conventional, e.g., *AnalySerie*-based methods (Paillard et
549 al. 1996) of stratigraphic correlation (Fig. S4). In turn, the hiatuses give intriguing new
550 insights into past changes of bottom current dynamics linked to different millennial-scale
551 geometries of overturning circulation and climate change such as in the South China Sea
552 (Sarnthein et al., 2013 and 2015), in the South Atlantic (Balmer et al. 2016) and southern
553 South Pacific (Ronge et al., 2019).
554
555 Clearly, the new 'rung ladder' of closely-spaced chronostratigraphic tie points has evolved
556 to a tool indispensable to uncover functional chains in paleoceanography, that actually
557 have controlled events of climate change over glacial-to-deglacial times.
558
559 *3.3 Definition and origin of Zoophycos burrows: A key foe of high-resolution stratigraphy*
560 *in Pleistocene sediment records turned into an ally?*
561



562 The *Zoophycos* producer displaces planktonic foraminifera tests, each marked by the
563 ^{14}C age of its shell formation, down to deep sediment levels, hence may severely bias
564 the faunal and isotopic composition and in particular, the ^{14}C age of the ambient host
565 sediment if (parts of) a *Zoophycos* burrow is picked in a sample. The well-defined 'rung
566 ladder' of ^{14}C plateaus defined in the host sediment now provides a clear yardstick both
567 for the relative chronostratigraphic displacement of the 'outlier' foraminiferal specimens
568 downcore in the host sediment and in particular, for the precise age of the source level
569 of these tests, that is the real time when a burrow was produced.

570

571 In continuation of previous studies (Löwemark and Grootes, 2004) Küssner et al.
572 (2018) demonstrated that *Zoophycos*-based vertical grain transport may reach down to
573 sediment depths of 150 cm. In particular, they showed that *Zoophycos* burrows formed
574 during brief episodes of enhanced burrowing activity that coincided with a marked drop
575 in sedimentation rate, that is, with events of reduced benthic nutrient supply. Thus the
576 "foe" *Zoophycos* may help corroborate reconstructed changes in climate and MOC.

577

578 *3.4 Empiric vs. model-based ^{14}C reservoir ages acting as tracer of past changes in*
579 *surface ocean dynamics and as incentive for further model refinements*

580

581 The tuning of ^{14}C plateau boundaries presents a technique unique to establish a suite
582 of highly resolved and robust age tie points on short and long time scales in ^{14}C -dated
583 marine sediment sections wherever retrieved in the global ocean (Fig. S2a). In
584 addition, and likewise intriguing, ^{14}C plateau tuning results in a suite of changing ^{14}C
585 reservoir ages over time, prime tracers of past oceanography of local surface waters
586 and a data set crucial to deduce past apparent deep-water ventilation ages (e.g.,



587 Muglia et al., 2018; Cook and Keigwin, 2015; Balmer and Sarnthein, 2018). Two
588 aspects help to sort out short-term climate-driven intra- and inter-plateau changes in
589 ^{14}C reservoir age, (i) the evaluation of individual reservoir ages is solely based on
590 judging a complete suite of plateaus, (ii) our experience shows that different climate
591 regimes in control of changes in surface ocean dynamics generally occurred on (multi-
592 millennial time scales (e.g., YD, B/A, HS-1), whereas atmospheric ^{14}C plateaus hardly
593 lasted longer than a few hundred up to ~ 1000 yr. Thus intra-plateau changes in ^{14}C
594 reservoir age are less likely, but indeed may amputate and/or deform a plateau to be
595 checked in detail for each suite of ^{14}C plateaus (Sarnthein et al., 2007, 2015).

596

597 To recap, the atmospheric ^{14}C plateaus of Suigetsu provide a suite of up to 18 reference
598 plateaus over the time span 10 – 29 cal. ka (Fig. 1). In marine sediment cores the ^{14}C
599 reservoir age of past surface waters is inferred from the difference between the average
600 ^{14}C age of an atmospheric ^{14}C plateau and that of a coeval ^{14}C plateau analyzed on
601 monospecific planktic foraminifera (Sarnthein et al., 2007). In low-to-mid latitudes our ^{14}C
602 records are based on *G. bulloides*, *G. ruber*, or *G. sacculifer* with habitat depths of 0–
603 80/120 (Jonkers and Kucera, 2017). In high latitudes, most ^{14}C records are derived from
604 *N. pachyderma* (s) living at 0–200 m depth (Simstich et al., 2003). Averaging of ^{14}C ages
605 within a ^{14}C plateau helps to bypass the analytical noise in ^{14}C records such as short-term
606 apparent ^{14}C age reversals and to deduce the regional evolution of planktic ^{14}C reservoir
607 ages with semi-millennial-scale resolution. Nine plateaus are located in the LGM, 18–27
608 cal. ka (Fig. 1). Here, plankton-based reservoir ages show analytical uncertainties of >200
609 to >300 yr each. By comparison, short-term temporal variations in reservoir age reach
610 200–400 yr, occasionally up to 600 yr, in particular, close to the end of the LGM (Table 3).

611



612 To better decode the informative value of LGM empiric ^{14}C reservoir ages we compare
613 them with estimates generated by a General Circulation Model (GCM) of ocean surface
614 waters (model of Muglia et al., 2018; 0–50 m w.d.; Fig. 7 and Suppl. Fig. S3d), an
615 approach similar to that of Toggweiler et al. (2019) applied to modern reservoir ages of the
616 global ocean. Low LGM values (300–750 yr) supposedly document an intensive exchange
617 of surface waters with atmospheric CO_2 , most common in model- and foraminifera-based
618 estimates of the low- and mid-latitude Atlantic. Low empiric values also mark LGM waters
619 in mid to high latitudes off Norway and off middle Chile, that is, close to sites of potential
620 deep and/or intermediate water formation. Off Norway and in the northeastern Atlantic,
621 model-based reservoir ages of Muglia et al. (2018) largely match the empiric range. This is
622 no proof yet for model quality, since the uncertainty envelopes (± 560 yr for data shown in
623 Fig. 7b; $r = 0.59$) generally far exceed the spatial differences calculated for the empiric
624 data. Contrariwise, model-based reservoir ages reproduce only poorly the low plankton-
625 based estimates off Central Chile and values in the Western Pacific and Southern Ocean.
626
627 In part, the differences may be linked to problems like insufficient spatial resolution along
628 continental margins and/or the estimates of a correct location and extent of seasonal sea
629 ice cover used as LGM boundary condition such as east off Greenland, in the subpolar
630 N.W. Pacific, and off Southern Chile, where sea ice hindered the exchange of atmospheric
631 carbon (per analogy to that of temperature exchange, as recorded by Sessford et al,
632 2019). In turn, model estimates are compared to ^{14}C signals of planktic foraminifera that
633 mostly formed during summer only, when large parts of the Nordic Seas were found ice-
634 free (Sarnthein et al., 2003). Hence, models may need to better constrain local and
635 seasonal sealing effects of LGM sea ice cover.

636



637 In general, however, the foraminifera-based reservoir age estimates for our sites that
638 represent various hydrographic key regions in the high-latitude ocean appear much higher
639 than model-derived values. Deviations reach up to 1400 yr, in particular in the Southern
640 Ocean. In part, the discrepancies may result from the fact that present models may not yet
641 be suited to capture values with great small-scale variability. Here, model-based reservoir
642 ages appear far too low in LGM regions influenced by regional upwelling such as the
643 South China Sea then governed by an estuarine overturning system (Wang et al., 2005;
644 Fig. 8), by coastal upwelling off N.W. Australia (Xu et al., 2010; Sarnthein et al., 2011), or
645 by a melt water lid such as off eastern New Zealand (Bostock et al., 2013; Küssner et al.,
646 2019, in prep.). Local oceanic features are likely to be missed in model simulation, for
647 example, by comparison to details in modern current geometry displayed by Yashayaev et
648 al. (2015) because of a model resolution still too coarse, a lack that suggests directions for
649 future model refinement. More narrow-spaced empiric data will help to weight more
650 correctly and develop the skill of models to capture past ^{14}C reservoir ages.

651

652 Various differences amongst plankton- and model-based reservoir ages may result from
653 differential seasonal habitats of the different planktic species analyzed that, in turn, may
654 trace different surface and subsurface water currents. Pertinent details are largely
655 unknown for the modern scenario because of the ‘bomb effect’, likewise no pertinent data
656 exist yet for the LGM. However, distinct interspecies differences were found in the
657 northern Norwegian Sea for the time span of the Preboreal ^{14}C plateau, 9.6–10.2 cal. ka
658 (Sarnthein and Werner, 2018). These differences amount up to 600 yr amongst paired ^{14}C
659 records of Arctic *Turborotalita quinqueloba* dominantly formed close to the sea surface
660 during peak summer, Arctic *Neogloboquadrina pachyderma* formed in subsurface waters,
661 and the subpolar species *N. incompta* mainly advected from the south by Norwegian



662 Current waters well mixed with the atmosphere during peak winter. This makes closer
663 specification of model results as product of different seasonal extremes a further target.
664

665 *3.5 Plankton-based ^{14}C reservoir ages – A prime database to estimate past changes in*
666 *the ^{14}C ventilation age of deep waters, ocean MOC, and DIC for past states of the ocean*
667

668 ‘Raw’ apparent benthic ventilation ages (in ^{14}C yr; ‘raw’ *sensu* Balmer et al., 2018) express
669 the difference between the (coeval) atmospheric and benthic ^{14}C levels measured at any
670 site and time of foraminifer deposition. These ages are the sum of (1) the planktic reservoir
671 age of the ^{14}C plateau that covers a group of paired benthic and planktic ^{14}C ages and (2)
672 the (positive or negative) ^{14}C age difference between any benthic ^{14}C age and the average
673 ^{14}C age of the paired planktic ^{14}C plateau. The benthic ventilation ages necessarily rely on
674 the high quality of ^{14}C plateau-based chronology, since the atmospheric ^{14}C level has been
675 subject to substantial short-term changes over glacial-to-deglacial times. Necessarily, the
676 ventilation ages include a mixing of different water masses that might originate from
677 different ocean regions and may contribute differential ^{14}C ventilation ages, an unknown
678 justifying the modifier ‘apparent’.

679
680 In a further step, the $\Delta\Delta^{14}\text{C}$ equivalent of our ‘raw’ benthic ventilation age may be adjusted
681 to changes in atmospheric ^{14}C that occurred over the (short) time span between deep-
682 water formation and benthic sediment deposition (e.g., Balmer and Sarnthein, 2018; Cook
683 and Keigwin, 2015). In most cases, however, this second step is omitted since its
684 application usually does not imply any major modification of the ventilation age estimates
685 (Fig. S4a; Skinner et al., 2017; Sarnthein et al., 2013).

686



687 On the basis of ^{14}C plateau tuning we now can rely on 18 precisely dated records of
688 apparent benthic ^{14}C ventilation ages (Fig. S4a-c) to reconstruct the global geometry of
689 LGM and HS-1 deep and intermediate water circulation as summarized in ocean transects
690 of Figs. 8 and 9. The individual matching of our 20 planktic ^{14}C plateau sequences with
691 that of the Suigetsu atmospheric ^{14}C record is displayed in Sarinthein et al. (2015), Balmer
692 et al., (2016), Küssner et al. (2019, in prep.), and Ausin et al. (2019, in prep.). In addition,
693 robust estimates of past reservoir ages are obtained for 4 planktic and benthic ^{14}C records
694 from paired atmospheric ^{14}C ages of wood chunks (Rafter et al., 2018; Zhao and Keigwin,
695 2018; Broecker et al., 2004).

696

697 *3.5.1 — Major features of ocean meridional overturning circulation during LGM (Fig. 9)*

698

699 Off Norway and near the Azores Islands very low benthic ^{14}C ventilation ages of <100–750
700 yr suggest ongoing deep-water formation in the LGM northern North Atlantic reaching
701 down to more than 3000–3500 m water depth, with a flow strength possibly similar to
702 today (and a coeval deep countercurrent of old waters from the Southern Ocean flowing
703 along the East Atlantic continental margin off Portugal). This pattern clearly corroborates
704 the assembled benthic $\delta^{13}\text{C}$ record showing plenty of elevated $\delta^{13}\text{C}$ values for the
705 northwestern, eastern and central North Atlantic (Sarinthein et al., 1994; Millo et al., 2006;
706 Keigwin and Swift, 2017). Irrespective of unspecified potential zonal variations in deep-
707 water ventilation age at mid latitudes and different from a number of published models
708 (e.g., Ferrari et al., 2014; Butzin et al., 2017) this ‘anti-estuarine’ pattern has been
709 confirmed by MIROC model simulations (Gebbie, 2014; Sherriff-Tadano et al., 2017,
710 Yamamoto et al., 2019) and, independently, by ϵ_{Nd} records (Howe et al., 2016; Lippold et
711 al., 2016). The latter suggest an overturning of AMOC possibly even stronger than today,



712 in particular due to a ‘thermal stronghold’ overlooked in other model simulations. Muglia et
713 al. (2018) tested in their model also a number of different AMOC flows with a strength of 6,
714 8, 9, and 13 Sv each, with estimates of 13 Sv appearing somewhat more consistent with
715 our results.

716

717 In contrast to the northern North Atlantic, North Atlantic Deep Waters and old Circumpolar
718 (CP) deep waters in the subpolar South Atlantic show an LGM ^{14}C ventilation age of
719 ~ 3640 yr, finally rising up to 4100 yr (Fig. 9). These waters were upwelled and admixed
720 from below to surface waters near to the sub-Antarctic Front during terminal LGM (Fig.
721 S4b; Skinner et al., 2010; Balmer and Sarinthein, 2016; model of Butzin et al., 2012).

722

723 In the southwestern South Pacific abyssal, in part possibly Antarctic-sourced waters (Rae
724 and Broecker, 2018) likewise show high apparent ^{14}C ventilation ages that rise from 3900
725 to 4800 yr over the LGM, in particular close to its end (Figs. 9 top and S4c) (^{14}C dates of
726 Ronge et al., 2016, modified by planktic ^{14}C reservoir ages of Küssner et al., 2019). A
727 vertical transect of benthic $\delta^{13}\text{C}$ (McCave et al., 2008) suggests that the abyssal waters
728 were overlain by CP waters, separated by pronounced stratification near $\sim 3500\text{--}4000$ m
729 water depth. In part, the CP waters stemmed from North Atlantic Deep Water. Probably,
730 their apparent ventilation age came close to 3900–4500 yr, similar to the values found in
731 the southern South Atlantic. East of New Zealand the CP waters entered the deep western
732 Pacific and spread up to the subpolar North Pacific, where LGM ^{14}C ventilation ages
733 reached 3700 yr.

734

735 Similar to today, the MOC of the LGM Pacific was shaped by estuarine geometry, probably
736 more weakened than today (Du et al., 2018) and more distinct in the far northwest than in



737 the far northeast. This geometry resulted in an upwelling of old deep waters in the
738 subarctic Northwest Pacific, here leading to a ^{14}C reservoir age of ~ 1700 yr for surface
739 waters at terminal LGM. On top of the Lower Pacific Deep Waters we may surmise Upper
740 Pacific Deep Waters that moved toward south (Fig. 9, top panel).

741

742 The Pacific deep waters were overlain by Antarctic / Pacific Intermediate Waters (IW) with
743 LGM ^{14}C ventilation ages as low as 1400–1600 yr, except for a shelf ice-covered site at
744 the southern tip of Chile with IW ages of 2460–3760 yr, possibly a result of local upwelling
745 of CP waters. In general, however, the low values of Pacific IW are similar to those
746 estimated for South Atlantic IW and likewise reflect a vivid exchange with atmospheric CO_2
747 in their source regions in the Southern Ocean (Skinner et al., 2015).

748

749 When entering and crossing the entrance sill to the marginal South China Sea the ‘young’
750 IW were mixed with ‘old’ CP waters entrained from below, here leading to ^{14}C ventilation
751 ages of 2600–3450 yr (Figs. 8 and S4d). The LGM South China Sea was shaped by an
752 estuarine-style overturning system marked by major upwelling near to its distal end in the
753 far southwest (Wang L. et al., 1999). This upwelling led to planktic ^{14}C reservoir ages as
754 high as 1200–1800 yr, values rarely found elsewhere in surface waters of low latitudes.

755

756 Our wide-spaced distribution pattern of 18 ^{14}C ventilation ages (plus 4 values based on
757 paired wood chunks) in Fig. 9 agrees only in part with the circulation patterns suggested
758 by the much larger datasets of ^{14}C ventilation ages compiled by Skinner et al. (2017) and
759 Zhao et al. (2018). Several features in Fig. 9 directly deviate, e.g., the ages we derive for
760 the North Atlantic and mid-depth Pacific. These deviations may be linked to both the
761 different derivation of our ^{14}C ventilation age estimates and the details of our calendar-year



762 chronology now based on the narrow-standing suite of ^{14}C plateau-boundary ages. The
763 quality of our ^{14}C reservoir ages of surface waters also controls the apparent ventilation
764 age of deep-waters, as it results from direct subtraction of a short-term ^{14}C average of an
765 atmospheric ^{14}C plateau from the paired benthic ^{14}C value, that is coeval with the planktic
766 ^{14}C plateau during the time of benthic foraminifera growth.

767

768 3.5.2 — Major features of meridional overturning circulation during early HS-1 (Fig. 9)

769

770 Near the onset of deglacial Heinrich Stadial 1 (HS-1; ~18–14.7 cal. ka) major shifts in ^{14}C
771 ventilation age suggest some short-lasting but fundamental changes in the circulation
772 geometry of the deep ocean, a central theme of marine paleoclimate research (Fig. 7,
773 lower panel of Fig. 9, and Figs. S2, S4a and b). Deep waters in the eastern Nordic Seas,
774 west of the Azores Islands, and off northern Brazil show a rapid rise to high ^{14}C ventilation
775 ages of ~2000–2500 yr and up to 4000 yr off Brazil, values that give first proof for a brief
776 switch from ‘anti-estuarine’ to ‘estuarine’ circulation that governed the central North
777 Atlantic and Norwegian Sea during early HS-1. This geometry continued – except for a
778 brief but marked and widespread event of recurring NADW formation near 15.2 ka – until
779 the very end of HS-1 near 14.5 ka (Fig. S4a; Muschitiello et al., 2019). The MOC switch
780 from LGM to HS-1 is in line with changes depicted in paired benthic $\delta^{13}\text{C}$ data (Sarnthein
781 et al., 1994), but not confirmed by the coeval ϵ_{Nd} record that suggests a constant source of
782 ‘mid-depth waters’, with the $\delta^{13}\text{C}$ drop being simply linked to higher ages (Howe et al.,
783 2018).

784

785 Conversely, benthic ^{14}C ventilation ages in the northeastern North Pacific (Site MD02-
786 2489) show a coeval and distinct but brief minimum of 1050-1450 yr near 3640 m w.d.



787 during early HS-1 (~18.1–16.8 ka; Figs. 9, S2, and S4d). This minimum was produced by
788 extremely small benthic-planktic age differences of 350–650 yr and provides robust
789 evidence for a short-lasting event of deep-water formation, that has flushed the north-
790 eastern North Pacific down to more than 3640 m w.d. (Gebhardt et al., 2008; Samthein et
791 al., 2013; Rae et al., 2014). Similar circulation geometries were reported for the Pliocene
792 (Burls et al., 2017). ‘Young’ Upper North Pacific Deep Waters (North Pacific Intermediate
793 Waters *sensu* Gong et al., 2019) then penetrated as ‘western boundary current’ far south,
794 up to the northern continental margin of the South China Sea (Fig. 8b and S4d). The short-
795 lasting North Pacific regime of anti-estuarine overturning was similar to that we find in the
796 modern and LGM Atlantic and, most interesting, simultaneous with its estuarine episode.
797
798 Recent data on benthic-planktic ^{14}C age differences (Du et al., 2018) precisely recover our
799 results at ~680 m w.d. off southern Alaska. However, they do not depict the ‘young’ deep
800 waters at their Site U1418 at ~3680 m w.d., as corroborated by a paired autigenic ϵ_{Nd}
801 maximum suggesting a high local bottom water age nearby. We assume that the amazing
802 difference in local deep-water ventilation ages is due to small-scale differences in the
803 effect of Coriolis forcing at high latitudes between a site located directly at the Alaskan
804 continental margin (U1418; Fig. 9b) and that on the distal Murray Sea Mount in the ‘open’
805 Pacific (MD02-2489; Fig. S4d), which has been washed by a plume of newly formed North
806 Pacific deep waters probably stemming from the Bering and/or Ochotsk Seas. In contrast,
807 the incursion of almost 3000 yr old deep waters from the Southern Ocean has continued
808 along the continental margin all over HS-1. In summary we may conclude that the
809 geometry of ocean MOC was briefly reversed in the ‘open’ North Pacific over almost 1500
810 years during HS-1, far deeper than suggested by previous authors (e.g., Okazaki et al.,



811 2012; Gong, S., et al. 2019), but similar to changes in geometry first proposed by Broecker
812 et al. (1985) then, however, for an LGM ocean.

813

814 3.5.3 — *Deep-Ocean DIC inventory*

815

816 Apart from the changing geometries in ocean MOC, the global set of ^{14}C plateau-based,
817 hence refined estimates of apparent ^{14}C ventilation ages (Fig. 9) has ultimately revealed
818 new insights into glacial-to-deglacial changes in the ocean DIC inventories (Sarnthein et
819 al., 2013). On the basis of GLODAP data (Key et al., 2004) any drop in ^{14}C concentration
820 (i.e., any rise in average ^{14}C ventilation age) of modern deep waters is tied linearly to a
821 rise of carbon (DIC) dissolved in deep ocean waters below ~ 2000 m, making for 1.22
822 micromole C / -1 ‰ ^{14}C . By and large, GCM and box model simulations of Chikamoto and
823 Abé-Ouchi (2012) and Wallmann et al. (2016) suggest that this ratio may also apply to
824 LGM deep-water circulation, when apparent ^{14}C ventilation ages in the Southern Ocean
825 increased significantly (from 2400 up to ~ 5000 yr) and accordingly, thermohaline
826 circulation was more sluggish and transit times of deep waters extended. Accordingly, a
827 'back-of-the-envelope' calculation of LGM ventilation age averages in the global deep
828 ocean suggests an additional carbon absorption of 730–980 Gt (Sarnthein et al., 2013).
829 This estimate can easily accommodate the glacial transfer of ~ 200 Gt C from the
830 atmosphere and biosphere, moreover, may also explain 200–450 Gt C then most probably
831 removed from glacial Atlantic and Pacific intermediate waters. These estimates offer an
832 independent evaluation of ice core-based data, other proxies, and model-based data on
833 past changes in the global carbon cycle (e.g., Menviel et al., 2018).

834

835 4. SOME CONCLUSIONS



836 – Regarding the upgraded Plateau-Tuning, despite some analytical scatter, ^{14}C ages for
837 the top and base of Lake Suigetsu-based atmospheric ^{14}C plateaus and coeval planktic
838 ^{14}C plateaus do not present statistical ‘outliers’ but real age estimates that are reproduced
839 by tree ring-based ^{14}C ages over the interval 10–13 cal. ka and further back.

840 – Hulu U/Th model-based ages of ^{14}C plateau boundaries of the Suigetsu atmospheric ^{14}C
841 record appear superior to those derived from microscopy-based varve counts only, since
842 U/Th model-based ages match far more closely the age deduced from XRF-based varve
843 counts for a crucial test case of lower plateau boundary 2b in the early deglacial, moreover,
844 the age assigned to the Laschamp event.

845 – During deglacial times, several ^{14}C plateaus paralleled a rise in air-sea gas exchange,
846 and, in turn, distinct changes in ocean MOC. By contrast, changes in cosmogenic ^{14}C
847 production rarely offer a complete explanation for the plateaus identified in the Suigetsu
848 ^{14}C data under discussion.

849 – In total, ^{14}C plateau boundaries in the range 29–10 cal. ka provide a suite of ~30 tie
850 points to establish – like chronological ladder rungs – a robust global age control for deep-
851 sea sediment sections and global stratigraphic correlations of last glacial to deglacial
852 climate events, 29–10 cal. ka. U/Th model ages confine the cal. age uncertainty of
853 Suigetsu plateau boundaries assigned halfway between two ^{14}C ages nearby inside and
854 outside a plateau’s scatter band to less than ± 50 – ± 70 yr.

855 – Regarding oceanographic implications, ^{14}C ages in a sediment section that form a
856 separate population of ^{14}C outliers clearly distinct from the ‘normal’ ^{14}C plateau suite help
857 to trace the reach and origin of Zoophycos burrows, a key ‘foe’ of high-resolution
858 stratigraphy in marine sediment cores, and allow for inferences on their origin in a major
859 reduction in sediment and nutrient supply.



860 – The difference in ^{14}C age between coeval atmospheric and planktic ^{14}C plateaus
861 presents a robust tracer of planktic ^{14}C reservoir ages and their temporal and spatial
862 variability, for the LGM and HS-1 now established for 18/20 sediment sites.
863 – Paired reservoir ages obtained from different planktic species document the local
864 distribution patterns of different surface water masses and prevailing foraminiferal habitats
865 at different seasons.
866 – A new, more reliable set of deep-water ^{14}C ventilation ages can be derived on the basis
867 of our robust planktic ^{14}C reservoir ages. These ventilation ages reveal geometries of LGM
868 overturning circulation, the main traits of which are similar to those of today. In contrast,
869 ^{14}C ventilation ages of early HS-1 suggest an almost 1500 yr long event of widely reversed
870 circulation patterns marked by deep-water formation and brief flushing of the northern
871 North Pacific and estuarine circulation geometry in the northern North Atlantic.
872 – Increased glacial ^{14}C ventilation ages and carbon (DIC) inventories of ocean deep
873 waters suggest an LGM drawdown of about 850 Gt C into the deep ocean and an early
874 deglacial abrupt carbon release to the atmosphere during HS-1 (Sarnthein et al., 2013).
875 – Comparison of planktic and model-based reservoir age estimates reveals some major
876 discrepancies, in particular at sites in middle to high latitudes, and points the way to further
877 model refinements to make the models better reflect the real complex patterns of ocean
878 circulation, including seasonality.

879

880 ACKNOWLEDGMENTS

881 We owe sincere thanks for plenty of stimulations to the 23rd International Radiocarbon
882 Conference in Trondheim, in particular to M.-J. Nadeau, and to the IPODS–OC3 workshop
883 in Cambridge U.K, 2018, convened by A. Schmittner and L. Skinner. Moreover, we thank
884 for most valuable basic discussions with R. Staff, Glasgow, J. Southon, Irvine CA, and M.



885 Butzin, AWI Bremerhaven, who kindly helped us to discuss the comparison of his model
886 results, and S. Beil, Kiel, for computer assistance. Over the last three years, G.
887 Mollenhauer measured with care hundreds of supplementary ^{14}C ages in her MICADAS
888 laboratory at AWI Bremerhaven. This study obtained long lasting special support from R.
889 Tiedemann and his colleagues at the AWI Bremerhaven.

890

891 **Author contribution**

892 All authors contributed data and valuable suggestions to write up this synthesis. MS
893 and PG designed the outline of this manuscript. KK, BA, TE and MS provided new
894 marine ^{14}C records in addition to records previously published. GS displayed the
895 details of Suigetsu varve counts. RM provided a ^{10}Be -based ^{14}C record and plots of
896 raw ^{14}C data sets of Suigetsu und Hulu Cave. Discussions amongst PG, RM, GS and
897 MS served to select U/Th-based model ages as best-possible time scale.

898

899 **Data availability**

900 Primary radiocarbon data of most sites are available at PANGAEA de, except for the
901 ^{14}C data of 5 marine cores still under publication by Küssner et al. and Ausin et al. (in
902 prep.; see caption of Fig. S4).

903

904 **REFERENCES (99)**

- 905 Adkins, J. F. and Boyle, E. A.: Changing atmospheric $\Delta^{14}\text{C}$ and the record of
906 paleoventilation ages. *Paleoceanography*, 12(3), 337–344, 1997.
- 907 Adolphi, F., Bronk Ramsey, C., Erhard, T., Lawrence Edwards, R., Cheng, H.,
908 Turney, C.S.M., Cooper, A., Svensson, A., Rasmussen, S.O., Fischer, H., and
909 Muscheler, R.: Connecting the Greenland ice-core and U/Th timescales via
910 cosmogenic radionuclides: testing the synchronicity of Dansgaard–Oeschger events.
911 *Clim. Past*, 14, 1755–1781. <https://doi.org/10.5194/cp-14-1755-2018>, 2018.
- 912 Alves, E.Q., Macario, K., Ascough, P., and Bronk Ramsey, C.: The worldwide
913 marine radiocarbon reservoir effect: definitions, mechanisms, and prospects. *Review of*
914 *Geophysics*, 56, <https://doi.org/10.1002/2017RG000588>, 2018.



- 915 Alveson, E.Q.: Radiocarbon in the Ocean, *EOS*, 99,
916 <https://doi.org/10.1029/2018EO095429>, 2018.
- 917 Ausin, B., Haghypour, N., Wacker, L., Voelker, A. H. L., Hodell, D., Magill, C., et al.:
918 Radiocarbon age offsets between two surface dwelling planktonic foraminifera species
919 during abrupt climate events in the SW Iberian margin. *Paleoceanography and*
920 *Paleoclimatology*, 34. <https://doi.org/10.1029/2018PA003490>, 2019.
- 921 Balmer, S., Sarnthein, M., Mudelsee, M., and Grootes, P. M.: Refined modeling and
922 ^{14}C plateau tuning reveal consistent patterns of glacial and deglacial ^{14}C reservoir
923 ages of surface waters in low-latitude Atlantic. *Paleoceanography*, 31.
924 <https://doi.org/10.1002/2016PA002953>, 2016.
- 925 Balmer, S. and Sarnthein, M.: Glacial-to deglacial changes in North Atlantic melt-
926 water advection and deep-water formation – Centennial-to-millennial-scale ^{14}C records
927 from the Azores Plateau. *Geochim. Cosmochim. Acta*, 236, 399-415,
928 <https://doi.org/10.1016/j.gca.2018.03.001>, 2018.
- 929 Berger W.H. and Keir, R.S.: Glacial-Holocene changes in atmospheric CO_2 and the
930 deep-sea record. J.E. Hansen, T. Takahashi (Eds.), *Geophysical Monograph*, 29,
931 American Geophysical Union, Washington, DC, pp. 337–351, 1984.
- 932 Bostock, H.C., Barrows, T.T., Carter, L., Chase, Z., Cortese, G., et al.: A review of
933 the Australian – New Zealand sector of the Southern Ocean over the last 30 ka (Aus-
934 INTIMATE project). *Quaternary Science Reviews* 74, 35-57, 2013.
- 935 Broecker W.S, Peteet, D.M., and Rind, D.: Does the ocean-atmosphere system have
936 more than one stable mode of operation? *Nature*, **315**, 21-26, doi:10.1038/315021a0,
937 1985
- 938 Broecker W.S., Barker, S., Clark, E., Hajdas, I., Bonani, G., and Stott, L.: Ventilation
939 of the Glacial deep Pacific Ocean, *Science*, 306, 1169–1172, 2004.
- 940 Bronk Ramsey, C., Staff, R. A., Bryant, C. L., Brock, F., Kitagawa, H., van der Plicht,
941 J., Scholout, G., Marshall, M. H., Brauer, A., Lamb, H. F., Payne, R. L., Tarasov, P. E.,
942 Haraguchi, T., Gotanda, K., Yonenobu, H., Yokoyama, Y., Tada, R., and Nakagawa,
943 T.: A complete terrestrial radiocarbon record for 11.2 to 52.8 kyr B.P., *Science*, 338,
944 370–374, 2012.
- 945 Bronk Ramsey, C. et al., *Radiocarbon*, (under review) 2019.
- 946 Burls, N.J., Fedorov, A.V., Sigman, D.M., Jaccard, S.L., Tiedemann, R., and Haug,
947 G.H.: Active Pacific meridional overturning circulation (PMOC) during the warm
948 Pliocene. *Sci. Adv.* 2017;3: e1700156, 2017.



- 949 Butzin, M., Prange, M., Lohmann, G.: Radiocarbon simulations for the glacial
950 ocean: The effects of wind stress, Southern Ocean sea ice and Heinrich events. *Earth*
951 *Planet. Sci. Lett.*, 235, 45-61, 2005.
- 952 Butzin, M., Prange, M., and Lohmann, G.: Readjustment of glacial radiocarbon
953 chronologies by self-consistent three-dimensional ocean circulation modeling. *Earth*
954 *Planet Sci. Lett.*, 317, 177-184, 2012.
- 955 Butzin, M., Köhler, P., and Lohmann, G.: Marine radiocarbon reservoir age
956 simulations for the past 50,000 years. *Geophys. Res. Lett.*, 44, 8473–8480,
957 doi:10.1002/2017GL074688, 2017.
- 958 Chen, T., Robinson, L.F., Burke, A., Southon, J., Spooner, P., Morris, P.J., and Ng,
959 H.C.: Synchronous centennial abrupt events in the ocean and atmosphere during the
960 last deglaciation, *Science*, 349, 1537-1541, 2015.
- 961 Cheng, H., Edwards, R.L., Southon, J., Matsumoto, K., Feinberg, J.M., Sinha, A.,
962 Zhou, W., Li, H., Li, X., Xu, Y., Chen, S., Tan, M., Wang, Q., Wang, Y., and Ning, Y.:
963 Atmospheric $^{14}\text{C}/^{12}\text{C}$ changes during the last glacial period from Hulu Cave, *Science*,
964 362, 1293-1297, 2018.
- 965 Chikamoto, M.O., Abé-Ouchi, A., Oka, A., Ohgaito, R., and Timmermann, A.:
966 Quantifying the ocean's role in glacial CO_2 reductions, *Climate of the Past*, 8, 545–563,
967 doi:10.5194/cp-8-545-2012, 2012.
- 968 Cook M.S. and Keigwin L.D.: Radiocarbon profiles of the NW Pacific from the LGM
969 and deglaciation: Evaluating ventilation metrics and the effect of uncertain surface
970 reservoir ages, *Paleoceanography*, 30, 174–195, 2015.
- 971 Davies, S.M., Davies, P.M., Abbott, Meara, R.H., et al.: A North Atlantic tephro-
972 stratigraphical framework for 130-60 ka b2k: New tephra discoveries, marine based
973 correlations, and future challenges, *Quaternary Science Rev.*, 106, 101-121, 2014.
- 974 Du, J., Haley, B.A., Mix, A.C., Walczak, M.H., and Praetorius, S.K.: Flushing of the deep
975 Pacific Ocean and the deglacial rise of atmospheric CO_2 concentrations, *Nature geoscience*,
976 11, 749-755, 2018.
- 977 Ferrari, R., Jansen, M.F., Adkins, J.F., Burke, A., Stewart, A.L., and Thompson,
978 A.F.: Antarctic sea ice control on ocean circulation in present and glacial climates, *Proc.*
979 *National Academy Science*, 111 (24), 8753–8758, 2014.
- 980 Gebbie, G.: How much did Glacial North Atlantic Water shoal? *Paleoceanography*,
981 29, 190-209, doi:10.1002/2013PA002557, 2014.



- 982 Gebhardt, H., Sarnthein, M., Kiefer, T., Erlenkeuser, H., Schmieder, F., and Röhl, U.:
983 Paleonutrient and productivity records from the subarctic North Pacific for Pleistocene
984 glacial terminations I to V. *Paleoceanography* 23, PA4212, 1-21,
985 doi:10.1029/2007PA001513, 2008.
- 986 Gong, S., Lembke-Jene, L., Lohmann, G., Knorr, G., Tiedemann, R., Zou, J.J and
987 Shi, X.F.: Enhanced North Pacific deep-ocean stratification by stronger intermediate
988 water formation during Heinrich Stadial 1. *Nature Communications*, 10: 656.
989 <https://doi.org/10.1038/s41467-019-08606-2>, 2019.
- 990 Grootes P.M. and Stuiver, M.: Oxygen 18/16 variability in Greenland snow and ice
991 with 1000 to 100000 year time resolution, *J. Geophys. Res.: Oceans* (1978–2012)
992 102(C12), 26455–26470, 1997.
- 993 Grootes, P.M. and Sarnthein, M.: Marine ¹⁴C reservoir ages oscillate, *PAGES News*,
994 14/3, 18-19, 2006.
- 995 Howe, J.N.W., Piotrowski, A.M., Noble, T.L., Mulitza, S., Chiessi, C.M., and Bayon,
996 G.: North Atlantic deep-water production during the last glacial maximum, *Nat.*
997 *Commun.*, 7, 11765, 2016. s
- 998 Howe, J.N.W., Huang, K-F., Oppo, D.W., Chiessi, C.M., Mulitza, S., Blusztajn, J.,
999 and Piotrowski, A.M.: Similar mid-depth Atlantic water mass provenance during the
1000 Last Glacial Maximum and Heinrich Stadial 1, *Earth Planetary Science Letters*, 490,
1001 51-61, 2018.
- 1002 Jonkers, L. and Kucera, M.: Quantifying the effect of seasonal and vertical habitat
1003 tracking on planktonic foraminifera proxies, *Climate of the Past*, 13, 573-586, 2017.
- 1004 Kawamura, K., Parrenin, F., Lisiecki, L., Uemura, R., Vimeux, F., Severinghaus,
1005 J.P., Hutterli, M.A., Nakazawa, T., Aoki, S., Jouzel, J., Raymo, M.E., Matsumoto, K.,
1006 Nakata, H., Motoyama, H., Fujita, S., Goto-Azuma, K., Fujii, Y., and Watanabe, O.:
1007 Northern Hemisphere forcing of climatic cycles in Antarctica over the past 360,000
1008 years, *Nature*, 448, 912-916, doi:10.1038/nature06015, 2007.
- 1009 Keigwin, L.D. and Swift, S.A.: Carbon isotope evidence for a northern source of
1010 deep water in the glacial western North Atlantic, *PNAS*, 114 (11), 2831-2835, 2017.
- 1011 Key R. M., Kozyr, A., Sabine, C.L., Lee, K., Wanninkhof, R., Bullister, J.L., Feely,
1012 R.A., Millero, F.J., Mordy, C., and Peng, T.-H. (2004) A global ocean carbon climat-
1013 ology: Results from Global Data Analysis Project (GLODAP), *Global Biogeochem. Cy.*,
1014 18, GB4031, doi:10.1029/2004GB002247, 2004.
- 1015 Kong, X., Wang, Y., Wu, J., Cheng, H., Edwards, R.L., and Wang, X.: Complicated



- 1016 responses of stalagmite $\delta^{13}\text{C}$ to climate change during the last glaciation from Hulu
1017 Cave, Nanjing, China, *Science in China Ser. D Earth Sciences*, 48, (12), 2174-2181,
1018 2005.
- 1019 Küssner, K., Sarnthein, M., Lamy, F., and Tiedemann, R.: High-resolution radiocarbon-
1020 based age records trace episodes of *Zoophycos* burrowing, *Marine Geology*, 403, 48-56,
1021 <http://doi:10.1016/j.margeo.2018.04.01>, 2018.
- 1022 Küssner, K., Sarnthein, M., Lamy, F., Michel, E., Mollenhauer, G., Siani G., and
1023 Tiedemann, R.: Glacial-to-deglacial reservoir ages of surface waters in the southern
1024 South Pacific, 2019 (in prep.).
- 1025 Lippold, J., Gutjahr, M., Blaser, P., Christner, E., de Cavalho-Fereira, M.L., Mulitza, S.
1026 et al.: Deep-water provenance and dynamics of the (de)glacial Atlantic meridional
1027 overturning circulation, *Earth Planetary Science Letters*, 445, 68-78, 2016.
- 1028 Lisiecki, L.E. and Stern, J.V.: Regional and global benthic $\delta^{18}\text{O}$ stacks for the last
1029 glacial cycle. *Paleoceanography*, 31, doi:10.1002/2016PA003002, 2016.
- 1030 Löwemark, L. and Grootes, P.M.: Large age differences between planktic
1031 foraminifers caused by abundance variations and *Zoophycos* bioturbation,
1032 *Paleoceanography*, 19, PA2001, doi:10.1029/2003PA000949, 2004.
- 1033 Marcott, S.A., Bauska, T.K., Buizert, C., Steig, E.J., Rosen, J.L., Cuffey, K.M.,
1034 Fudge, T.J., Severinghaus, J.P., Ahn, J., Kalk, M.L., McConnell, J.R., Sowers, T.,
1035 Taylor, K.C., White, J.W.C., and Brook, E.J.: Centennial-scale changes in the global
1036 carbon cycle during the last deglaciation, *Nature*, 514, 616-619,
1037 doi:10.1038/nature13799, 2014.
- 1038 Marshall, M., Scholaut, G., Brauer, A., Nakagawa, T., Staff, R.A., Bronk Ramsey,
1039 C., Lamb, H., Gotanda, K., Haraguchi, T., Yokoyama, Y., Yonenobu, H., Tada, R.,
1040 SG06 project members: A novel approach to varve counting using μXRF and X-
1041 radiography in combination with thin-section microscopy, applied to the Late Glacial
1042 chronology from Lake Suigetsu, Japan, *Quaternary Geochronology* 13, 70-80, 2012.
- 1043 McCave, I.N., Carter, I., and Hall, I.R.: Glacial-interglacial changes in water mass
1044 structure and flow in the SW Pacific Ocean, *Quaternary Science Rev.*, 27, 1886–1908,
1045 2008.
- 1046 Matsumoto, K.: Radiocarbon-based circulation age of the world oceans, *J. Geophys.*
1047 *Res.: Oceans* 112(C9), C09004. <https://doi.org/10.1029/2007JC004095>, 2007.
- 1048 Menviel, L., Spence, P., Yu, J., Chamberlain, M.A., Matear, R.J., Meissner K.J., and
1049 England, M.H.: Southern Hemisphere westerlies as a driver of the early deglacial



- 1050 atmospheric CO₂ rise, *Nature communications*, 9:2503, DOI:10.1038/s41467-018-
1051 04876-4, 2018.
- 1052 Millo, C., Sarnthein, M., and Erlenkeuser, M.: Variability of the Denmark Strait Overflow
1053 during the Last Glacial Maximum, *Boreas*, 35, 50-60, 2006.
- 1054 Muglia, J., Skinner, L., and Schmittner, A.: Weak overturning circulation and high
1055 Southern Ocean nutrient utilization maximized glacial ocean carbon, *Earth and*
1056 *Planetary Science Letters* 496, 47-56, 2018.
- 1057 Muschitiello, F., D'Andrea, W.J., Schmittner, A., Heaton, T.J., Balascio, N.L.,
1058 deRoberts, N., Caffee, M.W., Woodruff, T.E., Welten, K.C., Skinner, L.C., Simon, M.H.,
1059 and Dokken T.M.: Deep-water circulation changes lead North Atlantic climate during
1060 deglaciation, *Nature Communications* 10, 1272, doi.org/10.1038/s41467-019-09237-3,
1061 2019.
- 1062 Naughton, F., Costas, S., Gomes, S.D., Desprat, S., Rodrigues, T., Sanchez Goñi,
1063 M.F., Renssen, H., Trigo, R., Bronk-Ramsey, C., Oliveira, D., Salgueiro, E., Voelker,
1064 A.H.L., and Abrantes, F.: Coupled ocean and atmospheric changes during Greenland
1065 stadial 1 in southwestern Europe, *Quaternary Science Reviews*, 212, 108-120, 2019.
- 1066 Nydal R., Lovseth K., and Skogseth F. H.: Transfer of bomb ¹⁴C to the ocean
1067 surface, *Radiocarbon* 22(3), 626–635, 1980.
- 1068 Okazaki, Y., Sagawa, T., Asahi, H., Horikawa, K., and Onodera, J.: Ventilation
1069 changes in the western North Pacific since the last glacial period, *Climate of the Past*, 8,
1070 17-24, doi:10.5194/cp-8-17-2012, 2012.
- 1071 Paillard, D., Labeyrie, L., and Yiou, P.: Macintosh program performs time-series
1072 analysis, *Eos Trans, AGU*, 77: 379, 1996.
- 1073 Rae, J.W.B. and W. Broecker, W.: What fraction of the Pacific and Indian oceans'
1074 deep water is formed in the Southern Ocean? *Biogeosciences*, 15, 3779-3794, 2018.
- 1075 Rae, J., Sarnthein, M., Foster, G., Ridgwell, A., Grootes, P.M., and Elliott T.: Deep
1076 water formation in the North Pacific and deglacial CO₂ rise, *Paleoceanography*, 29,
1077 doi:10.1002/2013PA002570, 645–667, 2014.
- 1078 Rafter, P.A., Herguera, J.-C., and Southon, J.R.: Extreme lowering of deglacial
1079 seawater radiocarbon recorded by both epifaunal and infaunal benthic foraminifera in a
1080 wood-dated sediment core, *Climate of the Past* 14, 1977–1989, 2018.
- 1081 Reimer P.J., Bard, E., Bayliss, A., Beck, J. W., Blackwell, P.G., Bronk Ramsey, C.,
1082 Buck, C.E., Cheng, H., Edwards, R.L., and Friedrich, M.: IntCal13 and Marine13
1083 radiocarbon age calibration curves 0–50,000 years cal. BP, *Radiocarbon* 55, 1869–



- 1084 1887, 2013.
- 1085 Reimer, P.J., et al.: The IntCal19 northern hemisphere radiocarbon calibration curve
1086 (0-55 kcal BP), Radiocarbon, 2019 (under review).
- 1087 Ronge, T. A., Tiedemann, R., Lamy, F., et al.: Radiocarbon constraints on the extent
1088 and evolution of the South Pacific glacial carbon pool, Nature Communications 7:11487,
1089 2016.
- 1090 Ronge, T.A., Sarnthein, M., Roberts, J., Lamy, F., and Tiedemann, R.: East Pacific
1091 Core PS75/059-2: Glacial-to-deglacial stratigraphy revisited, Paleoceanography and
1092 Paleoclimatology, 34 (4), 432-435, DOI:10.1029/2019PA003569, 2019.
- 1093 Sarnthein, M., Winn, K., Jung, S.J., Duplessy, J.C., Labeyrie, L., Erlenkeuser, H.,
1094 and Ganssen, G.: Changes in east Atlantic deepwater circulation over the last 30,000
1095 years: eight time slice reconstructions, Paleoceanography, 9(2), 209–267, 1994.
- 1096 Sarnthein, M., Pflaumann, U., and Weinelt, M.: Past extent of sea ice in the
1097 northern North Atlantic inferred from foraminiferal paleotemperature estimates,
1098 Paleoceanography, 18(2), 2003.
- 1099 Sarnthein, M., Grootes, P.M., Kennett, J.P., and Nadeau, M.: ^{14}C Reservoir ages
1100 show deglacial changes in ocean currents and carbon cycle, Geophys. Monograph –
1101 Am. Geophys. Union, 173, 175–196, 2007.
- 1102 Sarnthein, M., Grootes, P.M., Holbourn, A., Kuhnt, W., and Kühn, H.: Tropical
1103 warming in the Timor Sea led deglacial Antarctic warming and almost coeval
1104 atmospheric CO_2 rise by >500 yr, Earth Planetary Science Letters, 302, 337-348, 2011.
- 1105 Sarnthein, M., Schneider, B., and Grootes, P.M.: Peak glacial ^{14}C ventilation ages
1106 suggest major draw-down of carbon into the abyssal ocean, Climate of the Past, 9 (1),
1107 925–965, 2013.
- 1108 Sarnthein, M., Balmer, S., Grootes, P.M., and Mudelsee, M.: Planktic and benthic
1109 ^{14}C reservoir ages for three ocean basins, calibrated by a suite of ^{14}C plateaus in the
1110 glacial-to-deglacial Suigetsu atmospheric ^{14}C record, Radiocarbon, 57, 129–151, 2015.
- 1111 Sarnthein, M. and Werner, K.: Early Holocene planktic foraminifers record species-
1112 specific ^{14}C reservoir ages in Arctic Gateway, Marine Micropaleontology, 135, 45-55.
1113 DOI:10.1016/j.marmicro.2017.07.002, 2018.
- 1114 Schlolaut, G.: A unique and easy-to-use-tool to deal with incompletely varved
1115 archives 782 – the Varve Interpolation Program 3.0.0, Quaternary Geochronology,
1116 2019 (in press).



- 1117 Schlolaut, G., Staff, R.A., Marshall, M.H., Brauer, A., Bronk Ramsey, C., Lamb,
1118 H.F., and Nakagawa, T.: Microfacies analysis of the Lake Suigetsu (Japan) sediments
1119 from ~50 to ~10 ka BP and an extended and revised varve based chronology,
1120 Quaternary Science Reviews, 200, 351-366, 2018.
- 1121 Schroeder, J., Holbourn, A., Küssner, K., and Kuhnt, W.: Hydrological variability in
1122 the southern Makassar Strait during the last glacial termination, Quaternary Science
1123 Reviews, 154, 143-156, 2016.
- 1124 Sessford, E.G., Jensen, M.F., Tisserand, A.A., Muschitiello, F., Dokken, T.,
1125 Nisancioglu, K.H., and Jansen, E.: Consistent fluctuations on intermediate water
1126 temperature off the coast off Greenland and Norway during Dansgaard-Oeschger
1127 events, Quaternary Science Reviews, 223, 105887, 1-17, 2019.
- 1128 Sherriff-Tadano, S., Abe-Ouchi, A., Yoshimori, M., Oka, A., and Chan, W.-L.:
1129 (Influence of glacial ice sheets on the Atlantic meridional overturning circulation through
1130 surface wind change, Climate Dynamics, 50 (7-8), 2881–2903, 2017.
- 1131 Siani, G., Michel, E., De Pol-Holz, R., DeVries, T., Lamy, F., Carel, M., Isguder, G.,
1132 Dewilde, F., Lourantou, A.: Carbon isotope records reveal precise timing of enhanced
1133 Southern Ocean upwelling during the last deglaciation, Nature Communications, 4,
1134 2758, 2013.
- 1135 Simstich, J., Sarnthein, M., and Erlenkeuser, H.: Paired $\delta^{18}\text{O}$ signals of
1136 *Neogloboquadrina pachyderma* (s) and *Turborotalita quinqueloba* show thermal
1137 stratification structure in Nordic Seas, Mar. Micropaleontol., 912, 1–19, 2003.
- 1138 Skinner, L.C., Fallon, S., Waelbroeck, C., Michel, E., and Barker, S.: Ventilation of
1139 the deep Southern Ocean and deglacial CO₂ rise, Science, 328, 1147–1151, 2010.
- 1140 Skinner, L.C., Waelbroeck, C., Scrivner, A.E., and Fallon, S.J.: Radiocarbon
1141 evidence for alternating northern and southern sources of ventilation of the deep
1142 Atlantic carbon pool during the last deglaciation, PNAS, 111, 5480–5484, 2014.
- 1143 Skinner, L.C. *et al.*: Reduced ventilation and enhanced magnitude of the deep Pacific
1144 carbon pool during the last glacial period, Earth and Planetary Science Letters, **411**, 45-
1145 52, 2015.
- 1146 Skinner, L.C., Primeau, F., Freeman, E., de la Fuente, M., Goodwin, P.A.,
1147 Gottschalk, J., Huang, E., McCave, I.N., Noble, T.L., and Scrivner A.E.: Radiocarbon
1148 constraints on the glacial ocean circulation and its impact on atmospheric CO₂, Nature
1149 communications, 8:16010, DOI: 10.1038/ncomms16010, 2017.



- 1150 Southon, J., Noronha, A.L., Cheng, H, Edwards, R.L., and Wang, Y.: A high-
1151 resolution record of atmospheric ^{14}C based on Hulu Cave speleothem H82, Quaternary
1152 Science Reviews, 33:32-41, 2012.
- 1153 Steffensen, J.P., Andersen, K.K., Bigler, M., et al.: High-Resolution Greenland Ice
1154 Core Data Show Abrupt Climate Change Happens in Few Years, Science, 321, 680;
1155 DOI: 10.1126/science.1157707, 2008.
- 1156 Stocker, T. and Johnsen, S.J.: A minimum thermodynamic model for the bipolar
1157 seesaw, Paleoceanography, 18 (4), 1087, doi:10.1029/2003PA000920, 2003.
- 1158 Stuiver, M. and Braziunas, T.V.: Modeling atmospheric ^{14}C influences and ^{14}C ages
1159 of marine samples to 10,000 B.C., Radiocarbon, 35, 137–189, 1993.
- 1160 Svensson, A., Andersen, K.K., Bigler, M., Clausen, H.B., Dahl-Jensen, D., Davies,
1161 S.M., Johnsen, S.J., Muscheler, R., Parrenin, F., Rasmussen, S.O., Röthlisberger, R.,
1162 Seierstad, I., Steffensen, J.P., and Vinther, B.M.: A 60 000 year Greenland
1163 stratigraphic ice core chronology, Climate of the Past, 4, 47–57, 2008.
- 1164 Toggweiler, J.R., Druffel, E.R.M., Key, R.M., and Galbraith, E.D.: Upwelling in the
1165 ocean basins north of the ACC. Part 2: How cool Subantarctic water reaches the surface
1166 in the tropics, J. Geophysical Research, DOI:10.1029/2018JC014795, 2019 (in press).
- 1167 Turney, C.S.M., Fifield, L.K., Hogg, A.G., et al.: Using New Zealand kauri (*Agathis*
1168 *australis*) to test the synchronicity of abrupt climate change during the Last Glacial
1169 Interval (60,000–11,700 years ago), Quatern. Sci. Rev., 29, 3677–3682, 2010.
- 1170 Turney, C.S.M., Jones, R.T., Phipps, S.J., et al.: Rapid global ocean-atmosphere
1171 response to Southern Ocean freshening during the last glacial, Nature communications,
1172 8:520, doi:10.1038/s41467-017-00577-6, 2017.
- 1173 Umling, N.E. and Thunnell, R.C.: Synchronous deglacial thermocline and deep-water
1174 ventilation in the eastern equatorial Pacific, Nature communications, 8, 14203. DOI:
1175 10.1038/ncomms14203, 2017.
- 1176 Waelbroeck, C., Duplessy, J.-C., Michel, E., Labeyrie, L., Paillard, D., and Duprat,
1177 J.: The timing of the last deglaciation in North Atlantic climate records, Nature, 412,
1178 724–727, 2001.
- 1179 Waelbroeck, C., Skinner, L.C., Labeyrie, L., Duplessy, J.-C., Michel, E., Riveiros,
1180 N.V., Gherardi, J.-M., and Dewilde, F.: The timing of deglacial circulation changes in
1181 the Atlantic, Paleoceanography, 26, PA3213, https://doi.org/10.1029/2010PA002007,
1182 2011.



- 1183 Wallmann, K., Schneider, B., and Sarnthein, M.: Effects of eustatic sea-level change,
1184 ocean dynamics, and nutrient utilization on atmospheric pCO₂ and seawater composition
1185 over the last 130,000 years – a model study, *Climate of the Past*, 12, 339-375, doi:
1186 10.5194/cp-12-339-2016, 2016.
- 1187 Wang Y.C, Cheng, H., Edwards, R.L., An, Z.S., Wu, J.Y., Shen, C.-C., and Dorale,
1188 J.A.: A high-resolution absolute-dated Late Pleistocene monsoon record from Hulu
1189 Cave, China, *Science*, 294, 2345- 2348. DOI: 10.1126/science.1064618, 2001.
- 1190 Wang, L.J., Sarnthein, M., Erlenkeuser, H., Grimalt, J., Grootes, P., Heilig, S., Ivanova,
1191 E., Kienast, M., Pelejero, C., and Pflaumann, U.: East Asian monsoon climate during the
1192 late Pleistocene: High-resolution sediment records from the South China Sea, *Marine*
1193 *Geology*, 156, 245-284, 1999.
- 1194 Wang, P., Clemens, S., Beaufort, L., Braconnot, P., Ganssen, G., Jian, Z., Kershaw,
1195 P., and Sarnthein, M.: SCOR/IMAGES Working Group 113 SEAMONS: Evolution and
1196 variability of the Asian Monsoon System: State of the art and outstanding issues,
1197 *Quaternary Science Reviews*, 24 (5-6), 595-629, 2005.
- 1198 Xu, J., Kuhnt, W., Holbourn, A., Regenberg, M., and Andersen, N.: Indo-Pacific
1199 Warm Pool variability during the Holocene and Last Glacial Maximum, *Paleoceanogr.*,
1200 25, 16, 2010.
- 1201 Yamamoto, A., Abe-Ouchi, A., Ohgaito, R., Ito, A., and Oka, A.: Glacial CO₂
1202 decrease and deep-water deoxygenation by iron fertilization from glaciogenic dust,
1203 *Climate of the Past*, 15, 981-996.
- 1204 Yashayaev, I., Seidov, D., and Demirov, E.: A new collective view of oceanography
1205 of the Arctic and North Atlantic basins, *Progress in Oceanography*, 132, 21 pp.,
1206 DOI:http://dx.doi.org/10.1016/j.pocean.2014.12.012, 2015.
- 1207 Zhao, N. and Keigwin, L.D.: An atmospheric chronology for the glacial-deglacial
1208 Eastern Equatorial Pacific, *Nature communications*, 9:3077, DOI:10.1038/s41467-018-
1209 05574-x, 2018.
- 1210 Zhao, N., Marchal, O., Keigwin, L., Amrhein, D., and Gebbie, G.: A synthesis of
1211 deep-sea radiocarbon records and their (in) consistency with modern ocean ventilation,
1212 *Paleoceanography and Paleoclimatology*, 33, 128-151, 2018.



1213 TABLE CAPTIONS

1214

1215 **✗ Table 1 a and b.** Summary of varve- and U/Th model-based age estimates (Schlolut
 1216 et al., 2018; Bronk Ramsey et al., 2012) for ~30 plateau (pl.) boundaries in the
 1217 atmospheric ¹⁴C record identified in Lake Suigetsu Core SG06₂₀₁₂ by means of visual
 1218 inspection over the interval 10.5–27 cal. ka (Sarnthein et al., 2015, suppl. and modified).
 1219 At the right hand side, three columns give the average (Ø) and uncertainty range of ¹⁴C
 1220 ages for each ¹⁴C plateau.

1221

SUIGETSU SG06_2012 Plateau no.	Plateau Top Varve-based age (yr BP)	U/Th-based age (yr BP)	Depth (cm c.d.)	Plateau Base Varve-based age (yr BP)	U/Th-based age (yr BP)	Depth (cm c.d.)	Ø 14C Age of 14C Plateau (14C yr)	±Uncertainty (14C yr)	14C age BP min/max. (1.6 σ range)
'Preboreal'	10525	10560	1325	11100	11108	1383	9525	–170/+110	9356/9635
'Top YD'	11290	11281	1402	11760	11755	1453	10060	–100/+35	9963/10095
'YD'	11950	11895	1467	12490	12475	1525	10380	–170/ 124	10211 10504
1a	13580	13656	1626	13980	14042	1657	12006	100	11857 12050
1	14095	14160	1666	15095	15100	1740	12471	185	12315 12683
2a	15310	15420	1754	16140	16520	1802	13406	245	13174 13665
2b	16075	16520	1802	16400	16930	1820	13850	40	13808 13885
3	16835	17500	1847	17500	18220	1888	14671	105	14582 14792
4	17880	18650	1913	18830	19590	1971	15851	190	15661 16044
5a	18960	19720	1978	19305	20240	2003	16670	90	16570

1222



									16750
5b	19305	20240	2003	20000	20900	2032	17007	190	16830 17247
6a	20190	21000	2050	20920	21890	2105	17667	262	17435 17960
6b	20920	21890	2105	21275	22300	2132	18075	140	17960 18240
7	21375	22400	2140	21790	22870	2171	18843	117	18741 18975
8	21835	22940	2175	22730	24250	2257	19715	-290 325	19425 20041
9	22730	24250	2257	23395	25150	2312	20465	-227 263	20238 20728
10a	23935	25880	2358	25080	27000	2400	22328	-380 270	21946 22600
10b	25080	27000	2400	25800	27600	2426	22708	-475 440	22233 23147
11	26110	27770	2443	27265	28730	2525	24088	-360 505	23727 24595

1223

1224

1225

1226

1227

1228

1229

1230

1231

1232

1233

1234

1235



1236 ✗ **Table 2.** Temporal match of ¹⁴C plateaus and deglacial periods of major degassing of
 1237 the ocean (AA = Antarctic).

DEGLACIAL EVENTS of pCO₂ RISE vs. age of pla. ¹⁴C PLATEAUS (in cal. ka)

pCO ₂ RISE (~12 ppm)	Plateau no.	Plateau boundaries	
AGE based on annual layers AA ice core		AGE (cal. ka) based on varve counts	U/Th model ages
(Marcott et al. 2014)		(Scholaut et al. 2018; Bronk Ramsey et al., 2012)	
11.7 – 11.5	# 'Top YD'	11.76 – 11.32	11.83 – 11.3
14.8 – 14.53	# 1	15.1 – 14.1	15.1 – 14.2
16.4 – 16.15	# 2a	16.14 – 15.3	16.52 – 15.5
17.4 – ~17.1	# 3	17.5 – 16.83	18.22 – 17.5

FURTHER POTENTIAL CORRELATIVES:

Progressive N. Atlantic warming during the YD at 12.39 – 12.03 ka *	# 'YD'	12.49 – 11.87	12.46 – 11.98
Onset of Antarctic ** warming at 18.3–17.6 ka (ice-based time scale)	#3	17.5 – 16.85	18.22 – 17.5
Onset of North Atlantic *** warming at 19.3–18.6 ka (U/Th-based time scale)	# 4	18.83 – 17.9	19.6 – 18.65
Top H2: GIS 2 N. Atlantic warming at 23.4 – 23.3 ka ****	#9 / #8	23.4 – 22.73	24.25 – 22.95

AGE CONTROL based on

- * Naughton et al. (2019)
- ** Kawamura et al. (2007)
- *** Balmer and Sarnthein (2018)
- **** Grootes and Stuiver (1997)

1238



1239 ✗ **Table 3** a-c. ¹⁴C reservoir / ventilation ages of surface (top 50-100 m) and bottom
 1240 waters vs. U/Th-based model age at 19/22 core sites in the ocean – (a) Spatial and
 1241 temporal changes over the LGM (22–20 and 20–18 cal. ka), (b) HS-1, and the B/A.
 1242 LGM estimates are compared to model-based estimates of Muglia et al. (2018). (c) Data
 1243 sources. For core locations see Fig. S2.
 1244 (a)

Sediment Core U/Th-based model age Plateau (Pl.) no.	Latitude	Longitude	Water depth (m)	LGM pla. res age		LGM model res. age		strong AMOC (yr)	weak (yr)
				24–21 ka Pl. 8 - 7 - 6 Error (yr)	21–18.7 ka Pl. 5 - 4/3 (yr, Error (yr))	21–18.7 ka Pl. 5 - 4/3 (yr, Error (yr))	21–18.7 ka Pl. 5 - 4/3 (yr, Error (yr))		
ATLANTIC O.									
PS2644	67°52.02'N	21°45.92'W	777	2100 ±390	1920–2200 ±325–±125	1920–2200 ±325–±125	1136	1100	
GIK 23074	66°66.67'N	4°90'E	1157	620–790 ±145–±270	550–1175 ±100–±200	550–1175 ±100–±200	1054	1059	
MD08-3180	38°N	31°13.45'W	3064	–	320–605 ±125–±405	320–605 ±125–±405	827	887	
SHAK06-5K (= MD99-2334)	37°34'N (37°48'N)	10°09'W 10°10'W	2646 3146	700–930	330–650	330–650	872	855	
ODP 1002	10°42.37'N	65°10.18'W	893	700–210 ±230–±310	25 – –205 ±205–±215	25 – –205 ±205–±215	751	738	
GeoB 3910-1	4°15'S	36°21'W	2361	–	–	–	779	796	
GeoB 1711-4	23°17'S	12°23'W	1976	1080 ±290	730–840 ±240–±190	730–840 ±240–±190	711	721	
KNR 159-5-36GG	27°31'S	46°48'W	1268	540 ±140	870 ±120	870 ±120	757	777	
MD07-3076	44°4'S	4°12'W	3770	–	2300 ±200	2300 ±200	928	989	
INDIAN O./TIMOR SEA									
MD01-2378	13°08.25'S	121°78.8'E	1783	–	2000–1700 ±300–±320	2000–1700 ±300–±320	885	890	
PACIFIC O.									
MD02-2489	54°39.07'N	148°92.13'V	3640	–	1560–1110 ±310–±335	1560–1110 ±310–±335	972	965	
MD01-2416	51°26.8'N	167°72.5'E	2317	–	1710 ±440	1710 ±440	1227	1202	
ODP 893A	34°17.25'N	120°02.33'V	588	–	1065 ±280	1065 ±280	839	846	
MD02-2503	34°16.6'N	120°01.6'W	580	–	–	–	839	846	
GIK 17940 (= SO50-37)	20°07.0'N 18°55'N	117°23.0'E 115°55'E	1727 2655	1820–1260 ±320–±230	hiatus	hiatus	836	838	
PS75/104-1 (= SO213-84)	44°46'S 45°7.5'S	174°31'E 174°34.9'E	835 972	1650–1280	1500	1500	881	895	
MD07-3088	46°S	75°W	1536	380	200-350	200-350	917	–	
SO213-76-2	46°13'S	178°1.7'W	4339	–	1600–1560	1600–1560	915	842	
PS97/137-1	52°39.5'S	75°33.9'E	1027	2290–2110	2400–1800	2400–1800	1505	1419	

1245
 1246
 1247
 1248
 1249
 1250
 1251
 1252



1253 (b)

Sediment Core U/Th-based model Plateau (Pl.) no.	HS-1 pla. res. age 18–16.5 ka		16.5–15.5 ka		B/A pla. res. age 14.7–13.6 ka		LGM be. vent age (yr)		LGM b.w. model age strong AMOC weak	
	Pl. 3 - 2b (yr)	Error (yr)	Pl. 2a (yr)	Error (yr)	Pl. 1 - 1a	Error (yr)	early	late	(yr)	(yr)
ATLANTIC O.										
PS2644	1775–1660	±105–±160	1900	±355	–	–	345	2400	948	918
GIK 23074	1730–2000	±125–±160	670	±310	140–310	±250–±100	375	375	960	931
MD08-3180	1420–1610	±310–±160	1460	±390	630–360	±310	600	600	1031	1004
SHAK06-5K (= MD99-2334)	350–420	–	550	–	800–1200	–	–	–	–	–
ODP 1002	–100 – 20	±140	90	±345	355	±200	–	–	2200–2700	1900
GeoB 3910-1	630–560	±160–±180	175	±475	210–230	±220–±110	2150	2150	1247	1175
GeoB 1711-4	660–690	±195–±45	420	±320	880	±255	1500	1500	1387	1714
KNR 159-5-36GGC	460–340	±380–±300	170	±700	180–230	±370–±310	1470	1470	1354	1563
MD07-3076	1650	±180	–	–	920	±230	3640	3640	1653	2060
INDIAN O./TIMOR SEA										
MD01-2378	740	±125	–	–	200–185	±345–±135	2720	–	1679	1881
PACIFIC O.										
MD02-2489	800–550	±155–±120	550	±305	440	±285	–	2625	2332	2595
MD01-2416	1480–1140	±135–±195	–	–	720–570	±285–±140	–	3700/510	2400	2683
ODP 893A	1065–1490	±280–±125	1400	±370	520	±185	–	1430	1677	1705
MD02-2503	965–1365	±160–±165	1215	±325	395–535	±240–±130	–	–	–	–
GIK 17940 (= SO50-37)	1210–1370	±200–±470	1045	±320	870–970	325–±100	3300–1800	–	1807	1897
PS75/104-1 (= SO213-84)	1050	–	1100	–	800–250	–	–	–	3225	3225
MD07-3088	800–1090	–	1010	–	730–940	–	1500	2400	1101	1146
SO213-76-2	200	–	–	–	–	–	1600	1600	1808	1701
PS97/137-1	1500–670	–	435	–	–	–	4685	4685	1712	2001
							3300	2100	1631	1871

1254

1255 (c)

Sediment Core	DATA Source
ATLANTIC O.	
PS2644	Samthein et al. 2015 Be. data suppl.
GIK 23074	Samthein et al. 2015
MD08-3180	Balmer et al. 2018
SHAK06-5K (= MD99-2334)	Ausin et al., 2019 Skinner et al. 2014
ODP 1002	Samthein et al. 2015
GeoB 3910-1	Balmer et al. 2016
GeoB 1711-4	Balmer et al. 2016
KNR 159-5-36GGC	Balmer et al. 2016 data suppl.
MD07-3076	Balmer et al. 2016
INDIAN O./TIMOR SEA	
MD01-2378	Samthein et al. 2015
PACIFIC O.	
MD02-2489	Samthein et al. 2015
MD01-2416	Samthein et al. 2015 modified
ODP 893A	Samthein et al. 2015 data suppl.
MD02-2503	Samthein et al. 2015
GIK 17940 (= SO50-37)	Samthein et al. 2015
PS75/104-1 (= SO213-84)	Küssner et al., 2018 Ronge et al., 2016
MD07-3088	Küssner et al., 2019
SO213-76-2	Küssner et al., 2019
PS97/137-1	Küssner et al., 2019

1256

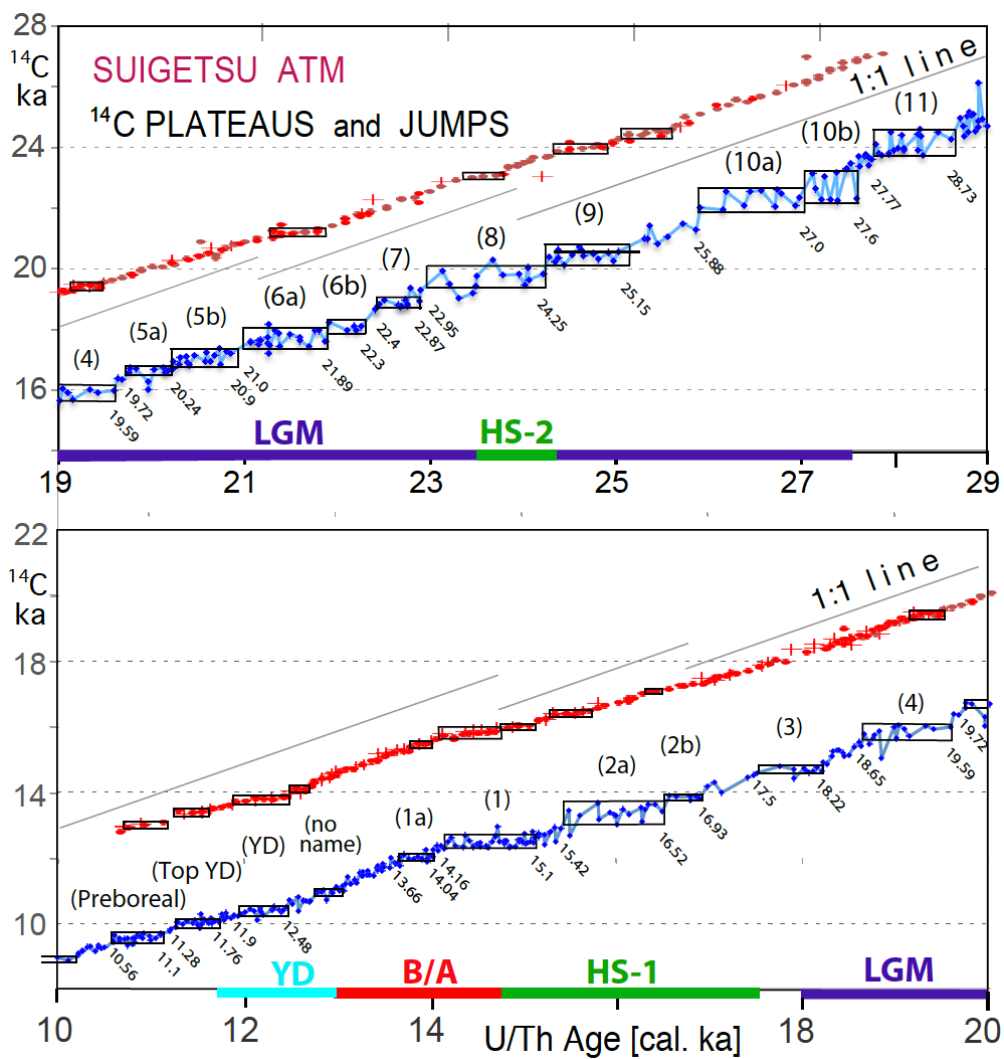
1257



1258 FIGURE CAPTIONS

1259

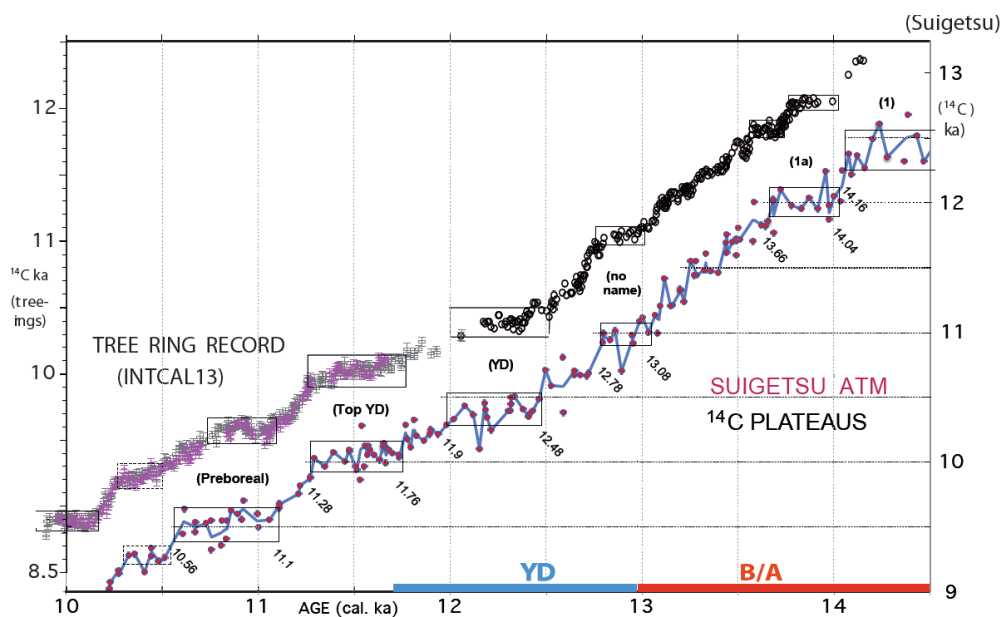
1260 – Fig. 1. Atmospheric ^{14}C ages of Lake Suigetsu plant macrofossils 10–29 cal. ka vs.
1261 U/Th-based model age (blue dots; Bronk Ramsey et al., 2012). Double and triple ^{14}C
1262 measurements are averaged. (In part large) error bars of single ^{14}C ages are given in
1263 Suppl. Fig. S1. Suite of labeled horizontal boxes that envelop scatter bands of largely
1264 constant ^{14}C ages shows ^{14}C plateaus longer than 250 yr (plateau boundary ages listed
1265 in Table 1). Red and brown dots (core samples from trench and wall) and + signs (off-
1266 axis core samples) depict raw ^{14}C ages of Hulu stalagmite core H82 (Cheng et al.,
1267 2018; Southon et al., 2012; plot offset by +3000 ^{14}C yr). Suite of short ^{14}C plateaus
1268 (black boxes) tentatively assigned to Hulu-based record occupy age ranges slightly
1269 different from those deduced for Suigetsu-based plateaus. The difference possibly
1270 results from short-term changes in the Old / Dead Carbon Fraction (ocf / dcf) that in turn
1271 may reflect major short-term changes in LGM and deglacial monsoon climate (Wang et
1272 al., 2001; Kong et al., 2005).



1273
 1274
 1275



1276 ✗ Fig. 2. High-resolution record of atmospheric ^{14}C jumps and plateaus (= suite of
1277 labeled horizontal boxes that envelop scatter bands of largely constant ^{14}C ages
1278 extending over >300 cal. yr) in a sediment section of Lake Suigetsu vs. tree ring-based
1279 ^{14}C jumps and plateaus 10–14.5 cal. ka (Reimer et al., 2013). Blue line averages paired
1280 double and triple ^{14}C ages of Suigetsu plant macrofossils. Age control points (cal. ka)
1281 follow varve counts (Schlolut et al., 2018) and U/Th model-based ages of Bronk
1282 Ramsey et al. (2012). YD = Younger Dryas, B/A = Bølling-Allerød.
1283



1284

1285

1286

1287

1288

1289

1290

1291

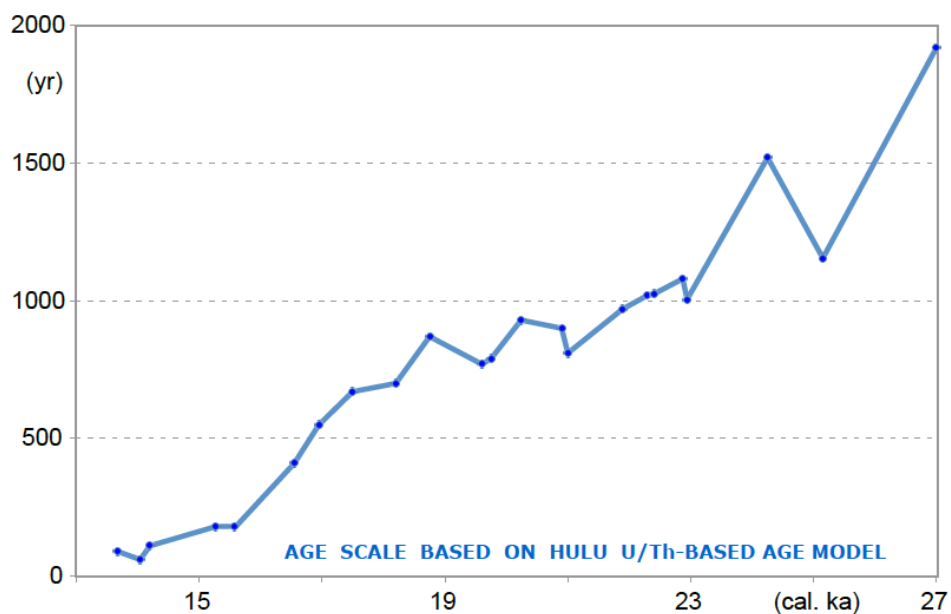
1292

1293

1294



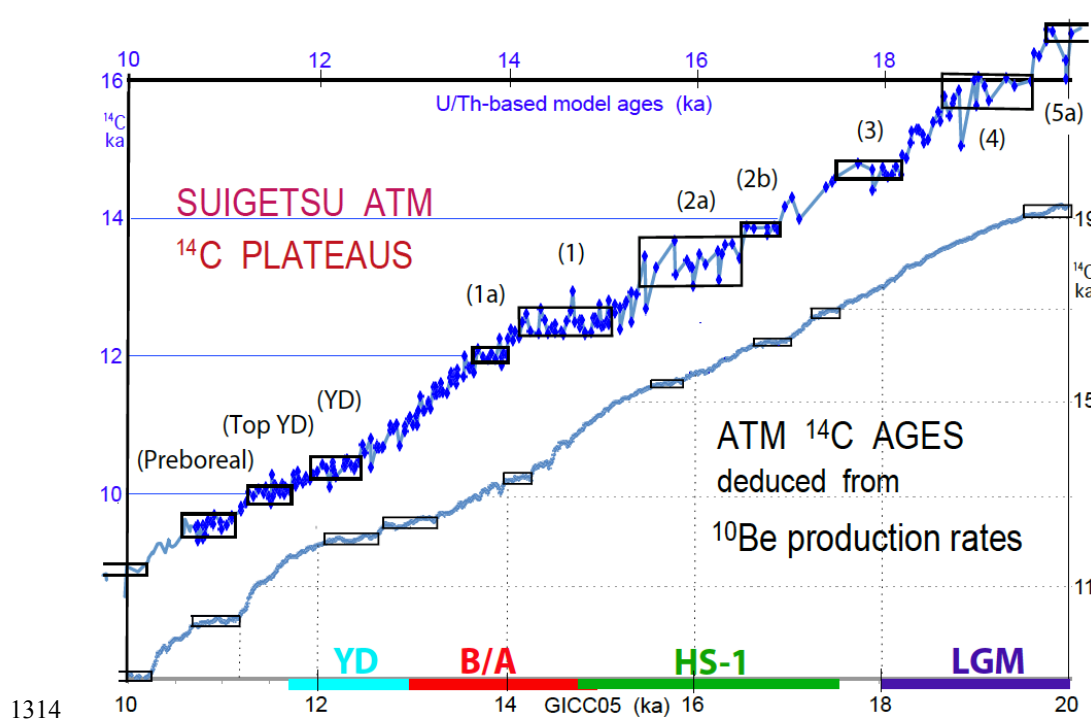
1295 ✗ Fig. 3. Difference between Hulu Cave U/Th-based model ages (Southon et al., 2012;
1296 Bronk Ramsey et al., 2012; Cheng et al., 2018) and varve count-based cal. ages for
1297 atmospheric ^{14}C plateau boundaries in Lake Suigetsu sediment record (Schlolut et al.,
1298 2018) (Sarnthein et al., 2015, suppl. and revised), displayed on the U/Th-based time
1299 scale 13–27 cal. ka.
1300

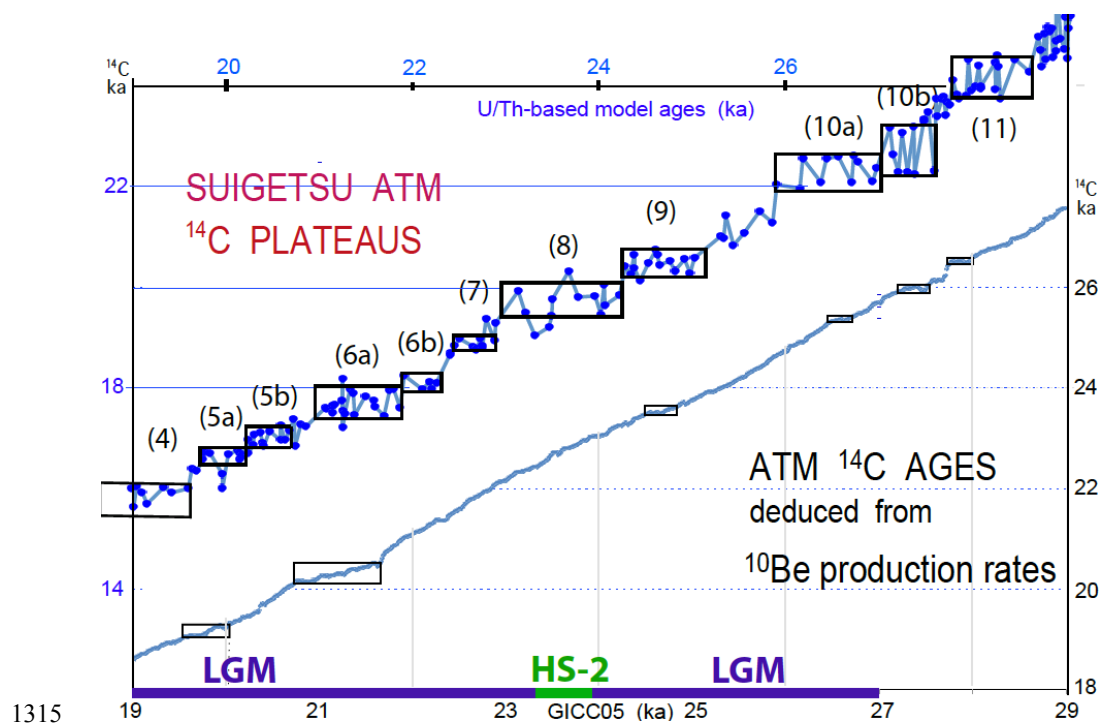


1301
1302
1303
1304
1305
1306
1307
1308
1309



1310 ✗ Fig. 4 a and b. Atmospheric ^{14}C ages and plateaus (horizontal boxes) deduced from
1311 ^{10}Be production rates vs. GICC05 age scale (Adolphi et al., 2018) compared to the
1312 Suigetsu record of atmospheric ^{14}C plateaus vs. Hulu U/Th-based model ages (Southon et
1313 al., 2012; Cheng et al., 2018).

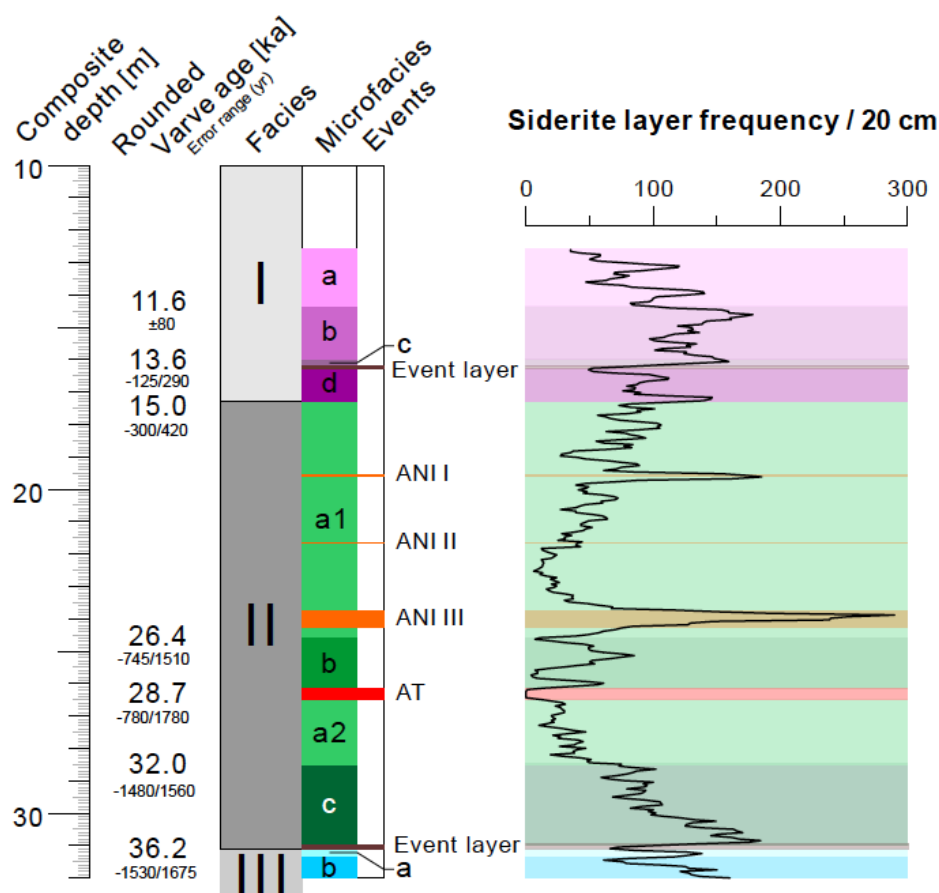




1315
1316
1317
1318
1319
1320
1321
1322
1323
1324
1325
1326
1327
1328



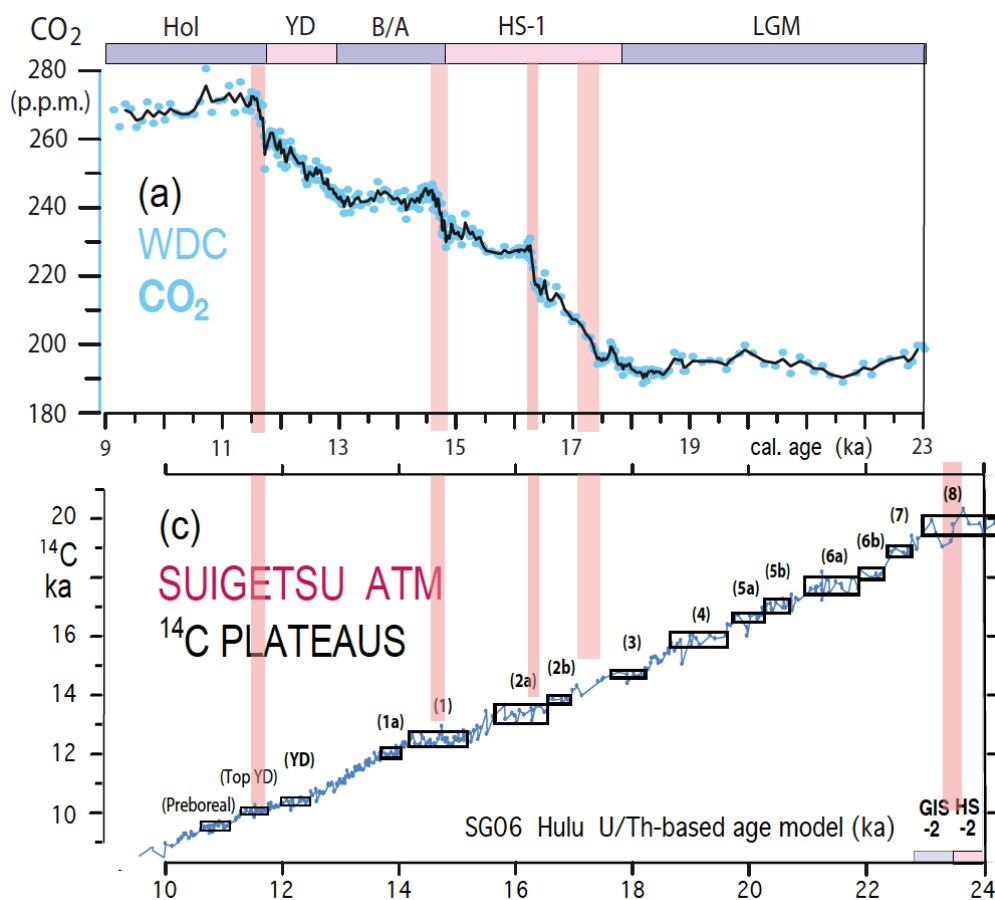
1329 ✗ Fig. 5. Sediment facies and microfacies zones in Lake Suigetsu Core SG06, ~13–32 m
 1330 depth (simplified and suppl. from Schlolaut et al., 2018). Microscopy-based frequency of
 1331 siderite layers with quality 1–3 in 20-cm sediment sections (= running average of layer
 1332 counts for 5 cm thick sections each), a measure of seasonal lamination quality with
 1333 gradual transitions between varved and poorly varved sediment sections. Rounded varve
 1334 ages are microscopy based and constrain age of major facies and microfacies
 1335 boundaries. ANI I to III mark core sections with ultrafine lamination due to sedimentation
 1336 rate minima, AT marks tephra layer named AT, ‘Event layers’ label major thin mud slides
 1337 probably earth quake-induced.



1338



1339 ✗ Fig. 6 (a). Four sudden steps (pink bars) in the deglacial atmospheric CO₂ rise at West
1340 Antarctic Ice Sheet Divide ice core (WDC) reflect events of fast ocean degassing, that may
1341 have contributed to the origin of deglacial ¹⁴C plateaus. Age control based on ice cores
1342 (Marcott et al., 2014). (b) The steps are compared to suite of atmospheric ¹⁴C plateaus dated
1343 by Hulu U/Th-based model ages (Bronk Ramsey et al., 2012). Hol = Holocene; YD = Younger
1344 Dryas; B/A = Bølling-Allerød; HS = Heinrich stadial; LGM = Last Glacial Maximum.
1345

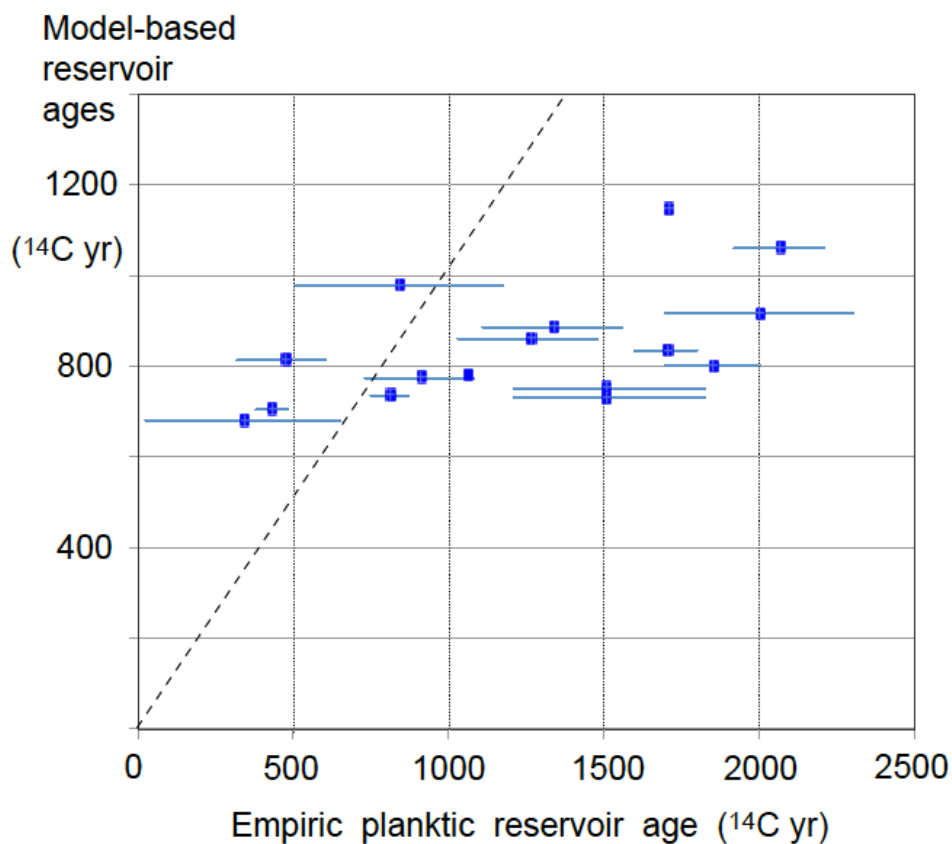


1346

1347



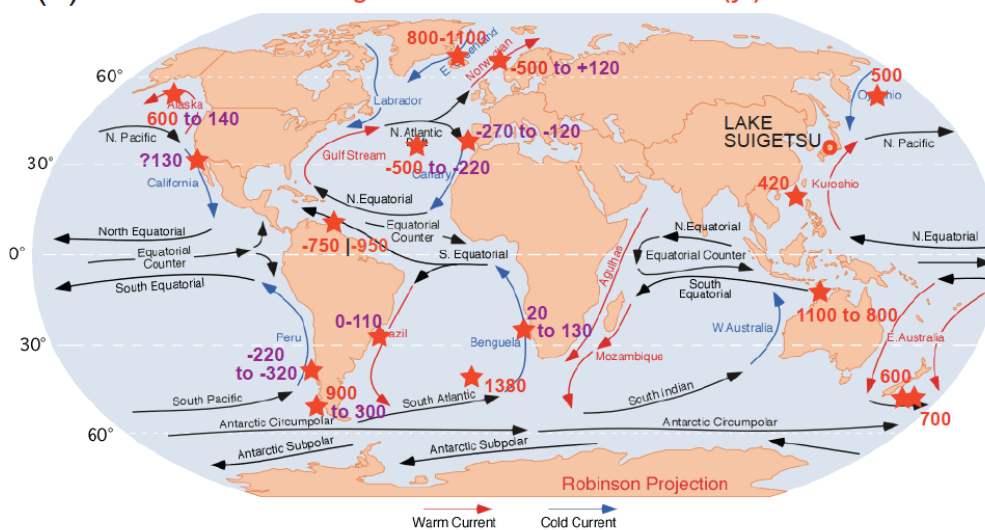
1348 ✗ Fig. 7. Global distribution of ^{14}C reservoir ages of Late LGM surface waters estimated
1349 by means of planktic ^{14}C plateau tuning and model-based estimates (general circulation
1350 model of Muglia et al., 2018), assuming an AMOC strength of 13 Sv). X-Y graph (a) and
1351 map (b) show (rounded) differences and intra-LGM trends with minor differences
1352 displayed in magenta, larger differences of >400 yr in red. Planktic habitat depths and
1353 model estimates are largely confined to 0–100 m water depth. Regional distribution
1354 patterns of LGM surface, intermediate, and deep-water ages are given in Table 3 and
1355 Suppl. Fig. S2.



1356



(b) **EMPIRIC minus Muglia MODEL RESERVOIR AGES (yr) of LGM S.W.**

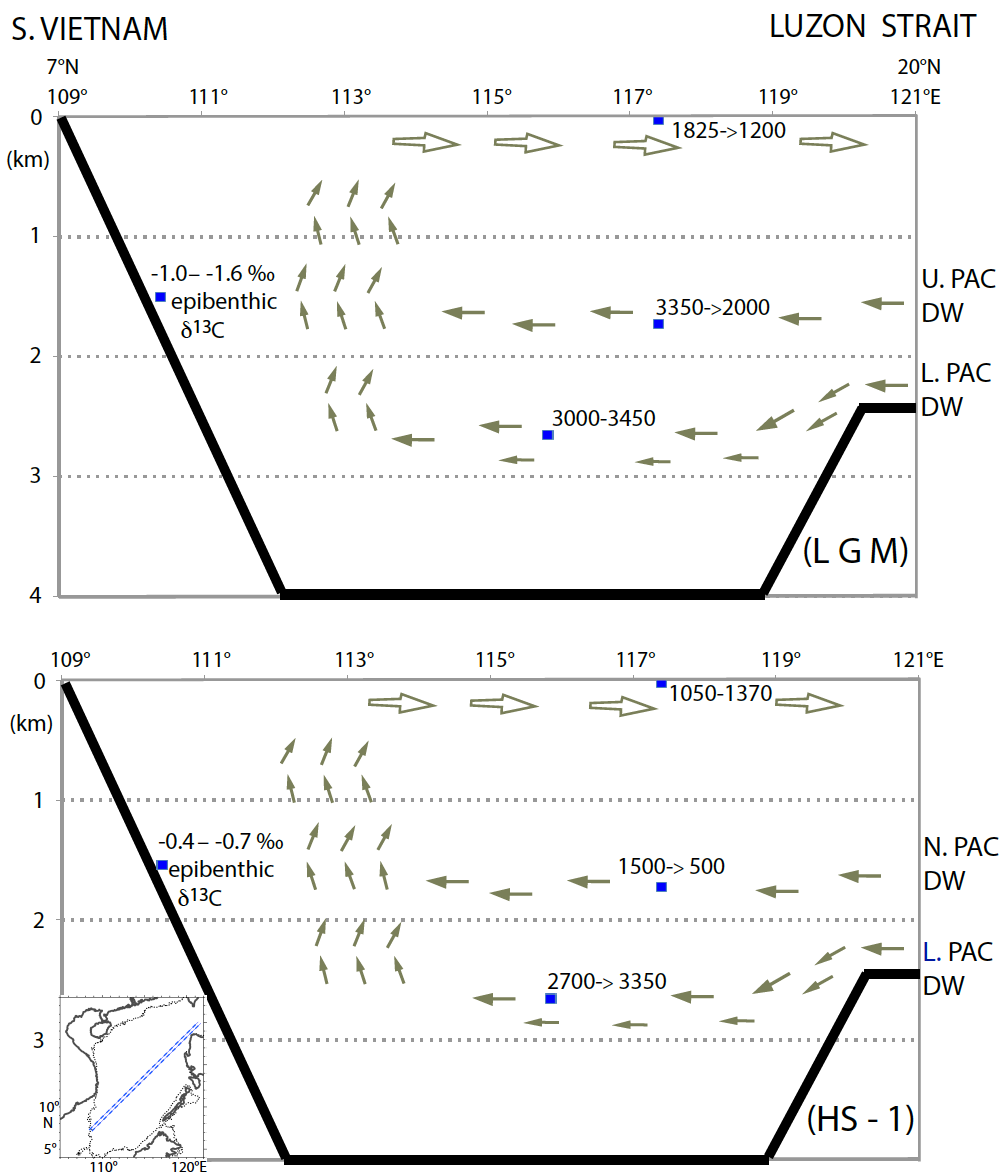


1357

1358

1359

1360 √ Fig. 8. SW–NE transect of ^{14}C reservoir and changes in ventilation ages across sites
1361 GIK17940 and SO50-37 in the South China Sea during late LGM (^{14}C Plateaus 5 and 4;
1362 upper panel) and HS-1 (lower panel). Insert map shows location of transect. Core
1363 locations are given in Fig. S2. An extreme epibenthic $\delta^{13}\text{C}$ minimum in far southwest
1364 (Core GIK17964; Sarnthein et al., 1999) reflects an LGM incursion of Lower/Upper
1365 Pacific Deep Waters (L./ U. PAC DW) with extremely high ^{14}C ventilation age and DIC
1366 enrichment in contrast to a low ventilation age of North Pacific Deep Water (N. PAC
1367 DW). Arrows reflect direction of potential deep and intermediate-water currents.



1368

1369

1370

1371

1372

1373



1374 ✗ Fig. 9. North Atlantic and North Pacific changes in benthic ^{14}C ventilation records reflect
1375 seesaw-style reversals in global MOC at the onset and end of early HS-1 (first proposed by
1376 Broecker et al., 1985, however, for LGM times). Arrows within numbers show temporal trends
1377 (a) Late LGM ocean transect reveals global MOC geometry largely similar to today. Blue and
1378 yellow arrows suggest average deep and intermediate-water currents that follow the gradient
1379 from low to high ventilation ages based on paired planktic ^{14}C reservoir ages derived by
1380 means of the ^{14}C plateau tuning technique (Sarnthein et al., 2013, Balmer et al., 2018,
1381 Küssner et al., 2019). Note major east-west gradient between LGM eastern and central
1382 Atlantic (off Portugal (PORT) vs. Mid-Atlantic Ridge W of Azores (MAR)). At some Pacific
1383 sites age control is based on paired ^{14}C ages of planktic foraminifera and wood chunks
1384 (marked by green 'w'; Sarnthein et al., 2015; Zhao and Keigwin, 2018, Rafter et al., 2018).
1385 Zigzag lines mark location of major frontal systems separating counter rotating ocean current:
1386 (e.g., W of Portugal and N of MD07-307: sensu Skinner et al., 2014). (b) HS-1 transect
1387 reveals a short-lasting Atlantic-style overturning in the subpolar North Pacific and a coeval
1388 Pacific-style stratification in the northern North Atlantic. Increased ventilation ages reflect an
1389 enhanced uptake of dissolved carbon in the LGM deep ocean (Sarnthein et al., 2013),
1390 sudden major drops suggest major degassing of CO_2 both from the deep Southern Ocean
1391 and North Pacific during early HS-1. SCS = South China Sea. – AABW = Antarctic Bottom
1392 Water; AAIW = Antarctic Intermediate Water. NADW = North Atlantic Deep Water. Blue
1393 arrows = high ventilation, yellow = poor ventilation, red arrows mark poleward warm surface
1394 water currents. Note many arrows are speculative using circumstantial evidence of benthic
1395 $\delta^{13}\text{C}$ records and likely local Coriolis forcing at high-latitude sites per analogy to modern
1396 scenarios. Location and names of sediment cores are given in Suppl. Fig. S2, short-term
1397 variations in planktic and benthic ^{14}C reservoir/ ventilation age in Suppl. Fig. S4 and Table 3.

